Acta Geologica Sinica (English Edition), 2019, 93(5): 1325–1353

Triassic Granitic Magmatism at the Northern Margin of the North China Craton: Implications of Geochronology and Geochemistry for the Tectonic Evolution of the Central Asian Orogenic Belt

CHEN Jingsheng[1], TIAN Dexin[2, *], YANG Hao[3], LI Weiwei[4], LIU Miao[1], LI Bin[1], YANG Fan[1], LI Wei[1] and WU Zhen[1]

[1] *Shenyang Geological Survey Center of China Geological Survey, Shenyang 110034, China*
[2] *Non-Ferrous Metals Geological Exploration Bureau of Zhejiang Province, Shaoxing, Zhejiang 312000, China*
[3] *College of Earth Sciences, Jilin University, Changchun 130061, China*
[4] *Institute of Geology and Mineral Resources of Liaoning Co., Ltd. Shenyang 110029, China*

Abstract: The early Mesozoic marked an important transition from collisional orogeny to post-orogenic extension at the northern margin of the North China Craton (NCC). In this study, we undertook zircon U-Pb dating and whole-rock major- and trace-element geochemical analyses of early Mesozoic granitic rocks in the Chifeng area to establish their geochronological framework, petrogenesis, and implications for the tectonic evolution of the eastern Central Asia Orogenic Belt (CAOB). Zircon U-Pb dating results show that these rocks were emplaced in three stages during the Triassic: (1) syenogranites during 250–248 Ma, (2) granodiorites during 244–243 Ma, and (3) monzogranites and granodiorites during 232–230 Ma. These Triassic granitoids belong to the high-K calc-alkaline series and are evolved I-type granites. They have high SiO_2 and low MgO contents with enrichments in light rare-earth elements, Zr, Hf, Rb, Th, and U, and depletions in Ba, Nb, Ta, Sr, and Eu. These geochemical data indicate that the granitoids were derived from partial melting of a lower-crustal source under relatively low-pressure conditions and subsequently underwent extensive fractional crystallization. Considering both the geochemical data and regional geological information, we propose that the 250–248 Ma syenogranites were emplaced in an extensional environment linked to slab break-off after closure of the Paleo-Asian Ocean (PAO) along the Solonker-Xra Moron-Changchun suture zone. The 244–243 Ma granodiorites were formed in a compressional orogenic setting during collision between the Erguna-Xing'an-Songliao composite block and the NCC. The 232–230 Ma granodiorites and monzogranites were emplaced during the transition from compressional orogeny to post-orogenic extension. Overall, the early Mesozoic tectonic evolution of the Chifeng area can be divided into three main stages: (1) closure of the Paleo-Asian Ocean and extension related to slab break-off during the Early Triassic; (2) continuous collisional compression during the Middle Triassic after closure of the PAO; and (3) post-orogenic extension during the Late Triassic, most probably due to lithospheric delamination after amalgamation of the Erguna-Xing'an-Songliao composite block and the NCC.

Key words: Triassic granitoids, zircon U-Pb geochronology, geochemistry, tectonic evolution, northern margin of the North China Craton

Citation: Chen et al., 2019. Triassic Granitic Magmatism at the Northern Margin of the North China Craton: Implications of Geochronology and Geochemistry for the Tectonic Evolution of the Central Asian Orogenic Belt. Acta Geologica Sinica (English Edition), 93(5): 1325–1353. DOI: 10.1111/1755-6724.14350

1 Introduction

The Central Asian Orogenic Belt (CAOB) is one of the largest accretionary orogens on Earth (Sengör et al., 1993; Windley et al., 2007) and lies between the two major continental blocks of the North China Craton (NCC) and the Siberian Craton (Mossakovsky et al., 1994; Sengör and Natal'in, 1996; Jahn et al., 2000; Buslov et al., 2001; Xiao et al., 2003, 2013; Jahn, 2004; Windley et al., 2007; Eizenhöfer et al., 2014; Song et al., 2016). The CAOB formed mainly from subduction of the Paleo-Asian oceanic plate and the amalgamation of terranes of different types and derivation (Sengör et al., 1993; Jahn et al., 2000; Xiao et al., 2003; Wu et al., 2011; Yang et al., 2019). The tectonic evolution of the CAOB is characterized by Paleozoic accretion, collision, and intracontinental deformation during closure of the Paleo-Asian Ocean (PAO) (Khain et al., 2002; Windley et al., 2007; Xiao et al., 2009; Wilhem et al., 2012; Xu et al., 2013; Li et al., 2015). However, the location of the suture that marks PAO closure and the timing of closure remain uncertain (Wang and Liu, 1986; Chen et al., 2000, 2009; Badarch et al., 2002; Xiao et al., 2003, 2009; Miao et al., 2007, 2008; Jian et al., 2008, 2010, 2012; Li et al., 2015; Dong et al., 2016; Yu et al., 2017; Tian et al., 2018). One school of

* Corresponding author. E-mail: 5202268@qq.com

thought is that the Hegenshan-Heihe suture represents the location of final closure of the ocean between the North China and Siberia cratons (Tang et al., 1990), but other researchers have argued that the final suture of the PAO is represented by the Solonker-Xra Moron-Changchun-Yanji suture (SXCYS) (Huang et al., 1977; Xiao et al., 2003; Sun et al., 2004). Since the proposal of these hypotheses, most paleontological, geochronological, sedimentary, and structural data have strongly supported the SXCYS as the final closure suture of the PAO (Xiao et al., 2003; Sun et al., 2004; Wu et al., 2007, 2011; Li Y L et al., 2009; Zhang et al., 2009a, b, c; Chen et al., 2009; Zhang X H et al., 2009a, b, 2012; Jian et al., 2010; Li et al., 2013, 2014, 2016a, b, 2017; Eizenhöfer et al., 2014, 2015a, b; Liu et al., 2015; Song et al., 2016; Yuan et al., 2016; Liu et al., 2017; Zhao et al., 2017; Yang et al., 2019). However, the closure time of the PAO along the SXCYS is much less certain, and the various proposals can be divided into the following five different viewpoints.

(1) On the basis of Sm-Nd isotopic data for mafic and ultramafic rocks from the Toudaogou Formation, as well as metamorphic data for the Hulan Group, it has been suggested that the PAO closed during the early Paleozoic and that the regional tectonic setting of the northern margin of the NCC changed from subduction to extension during the late Paleozoic (Zhao et al., 1996; Wang et al., 1997; Zhang et al., 1998).

(2) According to the analysis of sedimentary lithofacies and ophiolite mélanges, together with the contact relationship between Carboniferous strata and ophiolites, it has been proposed that the North China and Siberian cratons collided during the early late Paleozoic, accompanied by the closure of the PAO along the SXCYS. After the late Carboniferous, the Chifeng area was characterized by intracontinental rift magmatism and sedimentary deposition (He and Shao, 1983; Guo, 1986; Cao et al., 1986; Tang, 1990; Shao, 19991; Xu and Chen, 1997; Ren et al., 2002; Zhu, 2015), including formation of a rift basin during the Permian and associated intense volcanism related to tectonic extension (Tang, 1990; Shao, 1991).

(3) On the basis of the early to middle Permian alkaline granite belt distributed along the northern margin of the NCC, it has been inferred that the final closure time of the PAO along the SXCYS was sometime before the early to middle Permian (Shi et al., 2004; Zhang et al., 2007; Zhang X H et al., 2009a, b; Wang, 2014; Jiang, 2014; Li et al., 2016b).

(4) Considering observations of paleontological mixing and extinctions, detrital zircon U-Pb age data of Permian clastic sedimentary strata in the Balinzuoqi area, and paleomagnetic data (Wang and Liu, 1986; HsuÈ et al., 1991; Sengör et al., 1993; Li, 1995; Li et al., 2006, 2009; Zhang et al., 2009a; Zhang et al., 2015), it has been suggested that subduction of the Paleo-Asian oceanic plate continued during the late Paleozoic and finally ceased during the late Permian-Early Triassic. The following lines of evidence also support this proposal: 1) the Early Triassic magmatism occurred in a post-collision extensional environment (Xiao et al., 2003, 2009; Sun et al., 2004; Tang et al., 2004; Li, 2006; Zhang et al., 2006; Windley et al., 2007; Li et al., 2009; Zhang et al., 2009c; Li et al., 2013, 2014, 2016a, b, 2017); 2) Carboniferous ocean-floor basalts and Permian radiolarian siliceous rocks have been discovered to the north of the Xra Moron River, and late Permian reefs and marine fossils have been discovered in the Linxi area, underlying an unconformity in Baarin Right Banner and Jiutai County (Fan, 1996; Wang and Fan, 1997; Wang et al., 1999; Wang, 2001; Shang, 2004; Wang et al., 2005; Li et al., 2007); and 3) an island-arc/back-arc ophiolite suite formed during the late Permian-Early Triassic (Robinson et al., 1999; Miao et al., 2008; Jian et al., 2010; Chu et al., 2013; Song et al., 2016).

(5) The occurrence of middle Permian-Middle Triassic collisional granites and Late Triassic post-orogenic granites has been used to infer that closure of the PAO along the SXCYS started at the end of the late Permian but lasted through to the Late Triassic (Chen et al., 2001, 2002; Zhang et al., 2004; Li et al., 2007, 2009; Fu et al., 2010; Zhang et al., 2012; Sun, 2013; Duan et al., 2014; Liu et al., 2016).

The lack of consensus regarding the closure time of the PAO is partly because the distribution of magmatism between the northern margin of the NCC and the Xingmeng orogenic belt is unclear. There is also a need for data to be obtained from new research locations. The present study focuses on the less studied granitic intrusive rocks exposed in the Chifeng area, which connects the Songliao Block to the north with the NCC to the south. We present new zircon U-Pb ages and whole-rock major- and trace-element compositions for six early Mesozoic granitic plutons and evaluate their petrogenesis and tectonic environment. The results provide new evidence that constrains the closure time of the PAO.

2 Geological Background and Sample Descriptions

The North China-Inner Mongolia tract encompasses a vast area from southern Inner Mongolia to northern China along the central-eastern part of the CAOB (Fig. 1a). According to recent field observations, geochronology, geochemistry, and geophysics, three tectonic units have been recognized in this tract, including, from north to south, the Songliao Block, the northern margin of the NCC, and the NCC (Fig. 1; Wu et al., 2011)

The Songliao Block comprises the Mesozoic Songliao Basin, the Lesser Xing'an Range, and the Zhangguangcai Range. The Lesser Xing'an and Zhangguangcai ranges are characterized by voluminous Phanerozoic granitoids together with rare Paleozoic strata that occur as remnants in these granitoids (Wu et al., 2000, 2002). Data from several hundred drill-holes in the Songliao Basin reveal that Paleozoic-Mesozoic granitoids and Paleozoic strata (Gao et al., 2007; Pei et al., 2007) are widespread in the basement, with minor ~1.8 Ga Mesoproterozoic granitic gneisses (Wang et al., 2006; Pei et al., 2007) that may represent a tectonic slice of the NCC (Wu et al., 2011).

The southern core of the North China-Inner Mongolia tract, the NCC, is one of the most ancient cratons in the world, with crustal rocks as old as 3.8 Ga (Zhao and Zhai, 2013; Zhao, 2014). The craton features a basement of predominantly Archean-Paleoproterozoic tonalitic-

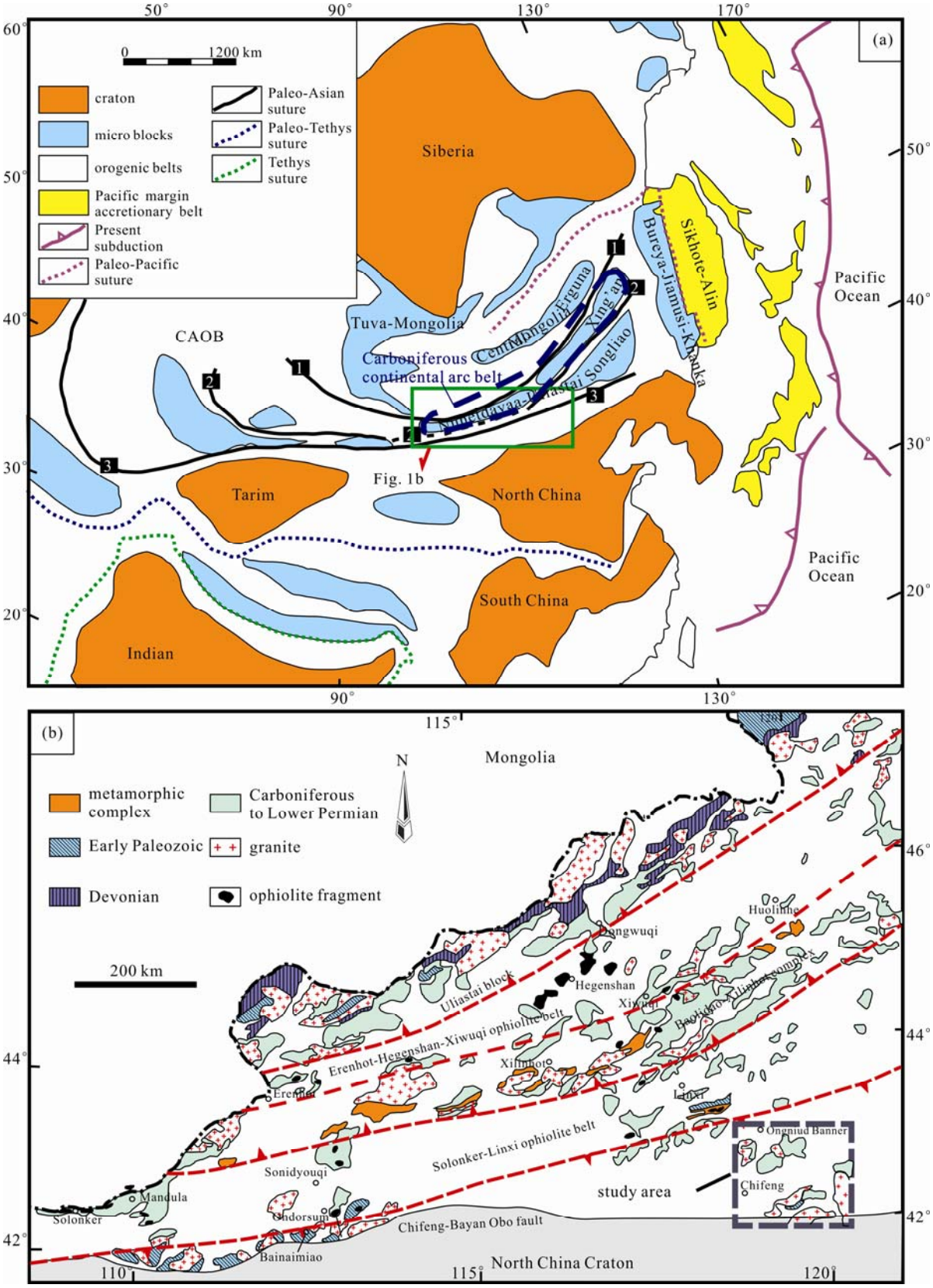

Fig. 1. (a) Schematic tectonic map showing main tectonic subdivisions of central and eastern Asia and location of northeast China (modified from Li, 2006); (b) geological map of the central Inner Mongolia of the CAOB showing tectonic units (modified from Song et al., 2015).

trondhjemitic-granodioritic (TTG) gneisses and meta-volcanic-meta-sedimentary rocks. Unconformably overlying the basement is a thick sequence of unmetamorphosed volcanic-sedimentary successions of Mesoproterozoic age, namely, the Changcheng, Jixian, and Qingbaikou systems, as well as Phanerozoic cover (Li et al., 1995; Zhao et al., 2005). Tectonically, the NCC is further divided into the Eastern and Western blocks and three Paleoproterozoic tectonic belts, which are the Khondalite Belt, the Jiao-Liao-Ji Belt, and the Trans-North China Orogen (Zhao and Guo, 2012). The Western Block is subdivided into the Yinshan Block in the north and the Ordos Block in the south, which amalgamated along the E-W-trending Khondalite Belt at ~1.95 Ga (Zhao et al., 2005; Guo et al., 2012). The Eastern Block is subdivided into the Langrim Block in the southeast and the Longgang Block in the northwest, which were joined along the Jiao-Liao-Ji Belt during the Paleoproterozoic (Li and Zhao, 2007). The united Eastern and Western blocks finally amalgamated along the Trans-North China Orogen at ~1.85 Ga (Zhao et al., 2005, 2008).

Extending from Chifeng through Faku and Liaoyuan to Yanji, the northern margin of the NCC was a convergent plate margin during the Paleozoic and was the site of episodic magmatic activity, including Devonian alkali intrusions, Carboniferous calc-alkaline intrusions and appinitic suites, early Permian mafic complexes and calc-alkaline granitoids, late Permian to Early Triassic calc-alkaline to alkaline intrusions, and Jurassic to Early Cretaceous granitoids (Zhang et al., 2009, 2010, 2011, 2012; Wu et al., 2011; Yu et al., 2014; Yuan et al., 2016).

The present study focuses on the Chifeng area around Chifeng City, Inner Mongolia Autonomous Region, situated within the northern margin of the NCC (Fig. 1). The units cropping out include (1) a Paleoproterozoic sedimentary-metamorphic assembly (e.g., the Baoyintu and Wulashan groups), which is composed of schist, marble, gneiss, and shallow granulite with a zircon U-Pb age of ca. 1860 Ma (Chen et al., 2015); (2) early Paleozoic marine-facies strata and intermediate to acidic volcanic rocks (e.g., the Cambrian Jinshan Formation, the Ordovician Minganshan Formation, and the Silurian Badangshan, Shaiwusu, and Xibiehe formations); (3) late Palaeozoic marine-facies strata (e.g., the Carboniferous Chaotugou, Baijiadian, and Jiujuzi formations, and the Permian Sanmianjing, Elitu, and Yujiabeigou formations), which are composed predominantly of limestone, marble, sandstone, and intermediate-basic volcanic rocks and have undergone slight metamorphism; and (4) Mesozoic terrigenous-facies volcanic-pyroclastic rocks and terrigenous clastic rocks (e.g., the Triassic Houfulongshan and Hongla formations, the Jurassic Manketouebo and Manitu formations, and the Cretaceous Baiyingaolao, Yixian, Jiufotang, Fuxin, and Sunjiawan formations).

Samples analyzed in this study were collected from six different Triassic granitic intrusions identified in the Chifeng area (Fig. 2), namely, the Mengguyingzi (MGYZ), Xiaxinjing (XXJ), Daluobogou (DLBG), Songshugouliang (SSGL), Ailingou (ALG), and Bajiazi (BJZ) plutons. Seven samples and 27 samples from these plutons were selected for geochronological and geochemical analyses, respectively.

The MGYZ pluton, located 5 km south of Aohan Banner (Fig. 2), intrudes Paleoproterozoic strata (i.e., the Baoyintu Group) and the Carboniferous Jiujuzi Formation, and is overlain by the volcanics and sediments of the Cretaceous Yixian Formation. This pluton is dominated by granodiorites (samples PM101-5-1, PM101-7-1, PM101-7-2, PM101-7-3, PM101-7-4, and PM101-7-5) with porphyritic texture and weak gneissosity. These samples consist of plagioclase (37 wt%), quartz (23 wt%), feldspar (5 wt%), hornblende (15 wt%), and biotite (15 wt%), with accessory zircon, titanite, magnetite, and apatite (5 wt%) (Fig. 3a, Fig. 3b). The pluton also contains a small amount of syenogranite (T101) (Fig. 2).

The XXJ pluton, located 50 km east of Chifeng City (Fig. 2), intrudes early Carboniferous granodiorites. Samples D2711-1, D2711-2, PM205-2-2, PM205-4-1, and PM205-10-1 are syenogranites with medium-fine-grained subhedral texture and massive structure. The main rock-forming minerals are alkali feldspar (50 wt%), quartz (35 wt%), plagioclase (10 wt%), and biotite (3 wt%), with accessory minerals including magnetite, zircon, and apatite (2 wt%) (Figs. 3c, 3d).

The DLBG pluton, located 15 km east of Heishui Town (Fig. 2), intrudes Permian monzogranite. Samples PM210-2-1, PM210-6-1, PM210-8-2, and PM210-8-3 are composed of syenogranite with medium-fine-grained subhedral texture and massive structure. The main rock-forming minerals are alkali feldspar (45 wt%), plagioclase (15 wt%), quartz (36 wt%), and biotite (2 wt%), with accessory minerals including apatite, titanium dioxide, zircon, and limonite (2 wt%) (Figs. 3e, 3f).

The SSGL pluton, located 17 km north of Heishui Town (Fig. 2), is intruded by Cretaceous monzogranite. This pluton is dominated by granodiorite (sample D3493-1) with medium-fine-grained subhedral texture and massive structure. The main rock-forming minerals are plagioclase (55 wt%), quartz (20 wt%), alkali feldspar (15 wt%), hornblende (5 wt%), and biotite (3 wt%), with accessory zircon, magnetite, and apatite (2 wt%) (Figs. 3g, 3h).

The ALG pluton, located 40 km north of Chifeng City (Fig. 2), intrudes the Silurian Badangshan, Shaiwusu, and Xibiehe formations. Samples 14CH13, 14CH14, 14CH15, 14CH16, and 14CH17 are granodiorites with medium-fine-grained texture and massive structure. They consist of plagioclase (50 wt%), quartz (22 wt%), alkali feldspar (15 wt%), and biotite (10 wt%), and accessory zircon, titanite, and apatite (3 wt%) (Figs. 3i, 3j).

The BJZ pluton, located 45 km southeast of Aohan Banner (Fig. 2), intrudes Permian monzogranite and is overlain by volcanics of the Cretaceous Yixian Formation. This pluton is dominated by monzogranites (samples PM403-3-1, PM403-5-1, PM403-7-1, PM403-7-2, M403-7-3, PM403-7-4, and PM403-7-5) with a fine-medium-grained granitic texture and massive structure. They consist of quartz (32 wt%), alkali feldspar (32 wt%), plagioclase (30 wt%), and biotite (5 wt%), and accessory zircon, hematite, pyrite, anatase, galena, and titanium dioxide (1 wt%) (Figs. 3k, 3l).

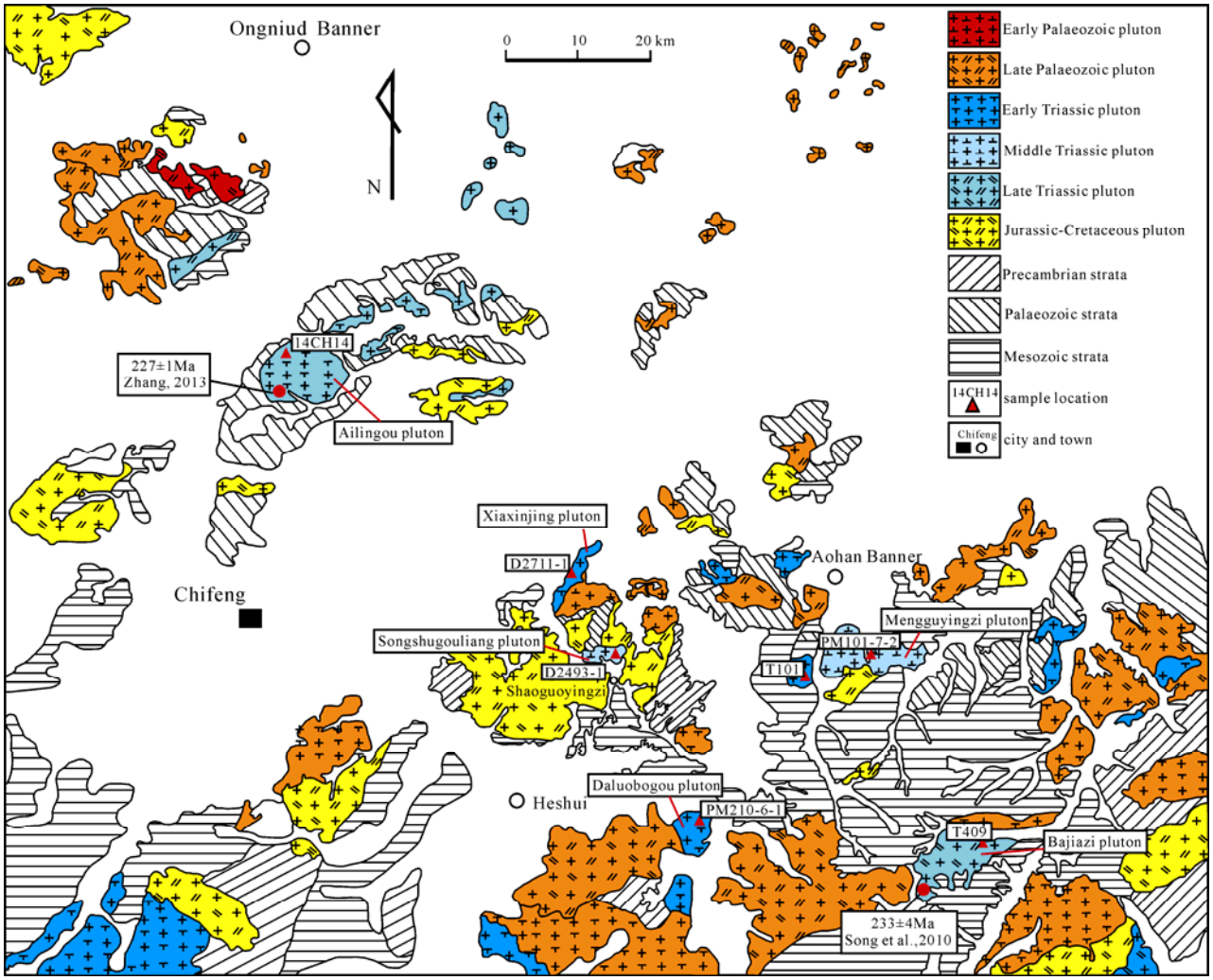

Fig. 2. A detailed geological map of the Chifeng City region in the north margin of the North China Craton showing sample locations, after the results of 1:50000 regional geological survey (2015).

3 Analytical Methods

3.1 Sample preparation

Zircons crystals were separated from whole-rock samples by using conventional heavy liquid and magnetic techniques, and the separates were further purified by hand-picking under a binocular microscope at the Langfang Yuneng Mineral Separation Limited Company, Hebei Province, China. The zircons were selected and embedded in epoxy resin and polished and then imaged using cathodoluminescence (CL) to reveal their internal structures with a scanning electron microscope. CL images of three samples (D2711-1, PM210-6-1, and D3493-1) were obtained at the electron microprobe Laboratory of the Institute of Geology and Geophysics, Chinese Academy of Sciences, and the others at the Zhongnan Mineral Supervision and Testing Center of the Ministry of Land and Resources.

3.2 Zircon LA-ICP-MS U-Pb isotope dating

U-Pb zircon ages for the Triassic granites in the Chifeng area were obtained using an Agilent 7500a inductively coupled plasma-mass spectrometry (ICP-MS) instrument equipped with a 193 nm ArF Excimer laser-ablation (LA) system. The spot size was 36 μm for the analyses, with an energy density of 8.5 J/cm^2 and a repetition rate of 10 Hz. Helium was used as the carrier gas to transport the ablated material from the standard LA cell. Zircon 91500 was used as the external standard for age calibration, and standard silicate NIST 610 glass was used to calibrate content calculations (Wiedenbeck et al., 1995). Zircon standards TEMORA (16±5 Ma) and QH (160±1 Ma) were also used as secondary standards to monitor any deviation of age measurement. Isotopic ratios and element contents were calculated using the Glitter software program. The age calculation and concordia plots were obtained using Isoplot (ver 3.0) (Ludwig, 2003). Common Pb was corrected using the method of Andersen (2002). Analyses of three samples (D2711-1, PM210-6-1, and D3493-1) were conducted at the Geologic Laboratory Center, China University of Geosciences (Beijing, China), and the others at the Zhongnan Mineral Supervision and Testing Center of the Ministry of Land and Resources.

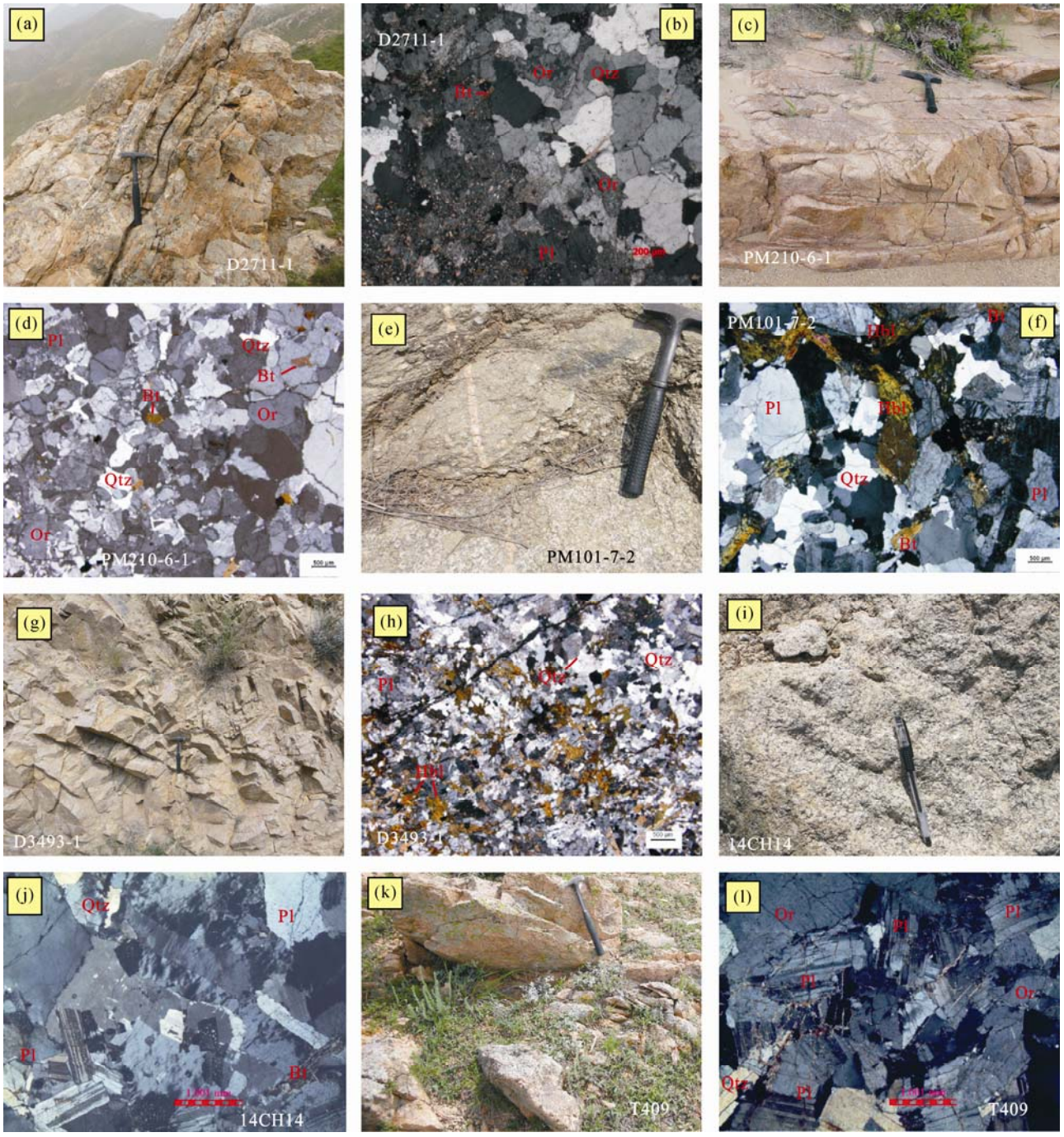

Fig. 3. Photographs and microphotographs (cross-polarized light) showing field relationships and rock textures.
(a) Outcrop of the Xiaxinjing syenogranite showing a massive structure; (b) Syenogranite (sample D2711-1); (c) Outcrop of the Daluotogou syenogranite showing a massive structure; (d) Syenogranite (sample PM210-6-1); (e) Outcrop of the Megnguyingzi granodiorite; (f) Granodiorite (sample PM101-7-2); (g) Outcrop of the Songshugouliang granodiorite; (h) Granodiorite (sample D3493-1);. (i) Outcrop of the Ailingou granodiorite showing a medium-fine grained texture; (j) Granodiorite (sample14CH14); (k) Outcrop of the Bajiazi monzogranite showing a massive structure; (l) Monzogranite (sampleT409).

3.3 Major- and trace-element analyses

Major-, trace-, and rare-earth-element (REE) analyses for 29 samples were performed at the Northeast China Supervision and Inspection Center of Mineral Resources, Ministry of Land and Resources, Shenyang, China. Samples were crushed and ground to 200 mesh in an agate mill after petrographic examination and removal of altered rock surfaces. Whole-rock major-element contents were determined by X-ray fluorescence spectrometry (XRF), yielding analytical precisions of better than 2%. Trace-element and REE contents were determined by ICP-MS, and yielding analytical precisions of better than 5% for elements with contents of >10 ppm, better than 8% for elements with contents of <10 ppm, and 10% for the

transition metals. Details of the techniques used for major- and trace-element determinations are described by Li et al. (2005).

4 Analytical Results

4.1 Zircon U-Pb ages

Seven granite samples were selected for zircon LA-ICP-MS dating, and the analytical results are listed in Table 1. All the zircons are transparent and generally euhedral, ranging in size from 80 to 200 μm with length:width ratios of 1:1 to 3:1. Almost all of these zircons are pure, colorless, and euhedral-subhedral and contain clear oscillatory zoning visible during CL imaging (Fig. 4). These features, in combination with high Th/U ratios of 0.20–5.90, indicate a magmatic origin (Hoskin et al., 2001; Belousova et al., 2002). Therefore, the ages represent the timing of crystallization of these samples. Zircon U-Pb concordia diagrams with weighted mean ages are shown in Fig. 5.

4.1.1 Early Triassic syenogranite

Sample D2711-1 is a syenogranite from the Xiaxinjing pluton. Twenty-four U-Pb analyses were obtained, with all but three yielding ages of 260 to 242 Ma distributed in one group on or near the concordia. Their weighted mean $^{206}Pb/^{238}U$ age is 250±2 Ma (MSDW=1.5; n=21) (Fig. 5a), which is regarded as the crystallization age of sample D2711-1.

Sample T101 is a syenogranite from the Mengguyingzi pluton. Twenty U-Pb analyses were obtained, with all but one yielding ages of 255 to 234 Ma clustered in a single group on or near the concordia. Their weighted mean $^{206}Pb/^{238}U$ age is 250±4 Ma (MSDW=0.59; n=19) (Fig. 5b), which is interpreted to represent the crystallization age of the syenogranite.

Sample PM210-6-1 is a syenogranite from the Daluobogou pluton. Twenty-five U-Pb analyses were obtained, with all but one of the ages ranging from 253 to 244 Ma distributed in a group on or near the concordia. Their weighted mean $^{206}Pb/^{238}U$ age is 248±1 Ma (MSDW=0.87; n=24) (Fig. 5c) and is interpreted as the crystallization age of the syenogranite.

4.1.2 Middle Triassic granodiorite

Sample PM101-7-2 is a granodiorite from the Mengguyingzi pluton. Twenty U-Pb analyses were obtained, of which all but two data give a range of $^{206}Pb/^{238}U$ ages between 255 and 238 Ma and are clustered in a single group on or near the concordia. Their weighted mean $^{206}Pb/^{238}U$ age is 244±2 Ma (MSDW=0.78; n=18) (Fig. 5d), which is regarded as the crystallization age of sample PM101-7-2.

Sample D3493-1 is a granodiorite from the Songshugouliang pluton. Twenty-five U-Pb analyses were obtained, with all but four giving a range of $^{206}Pb/^{238}U$ ages between 247 and 236 Ma and being distributed in one group on or near the concordia. Their weighted mean $^{206}Pb/^{238}U$ age is 243±1 Ma (MSDW=0.66; n=21) (Fig. 5e), which is interpreted as representing the timing of crystallization of the granodiorite.

4.1.3 Late Triassic granodiorite and monzogranite

Sample 14CH14 is a granodiorite from the Ailingou

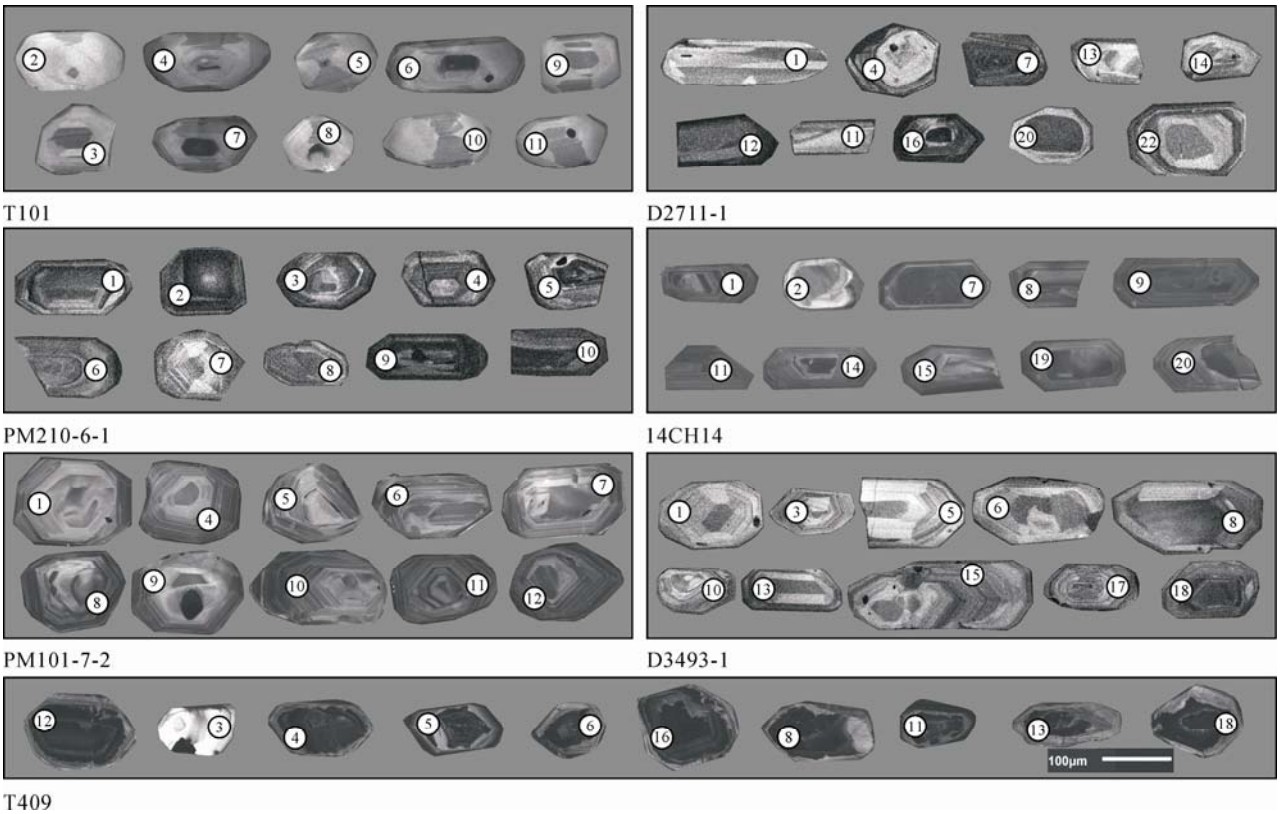

Fig. 4. Cathodoluminescence (CL) images of selected zircon grains from Triassic granites in this study.

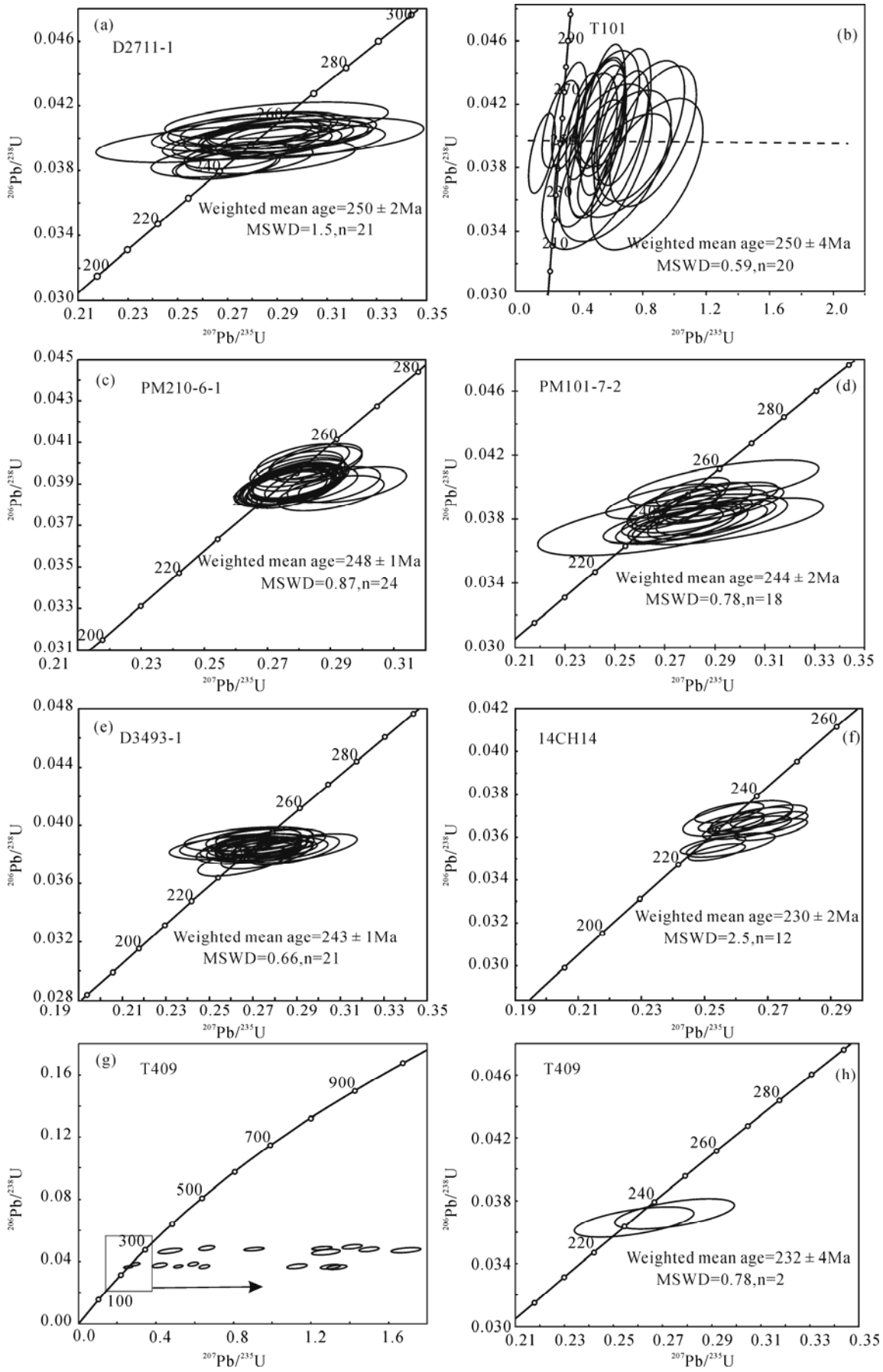

Fig. 5. Zircon $^{207}Pb/^{235}U$-$^{206}Pb/^{238}U$ concordia diagrams of Triassic granites samples from this study.

Table 1 LA-ICP-MS zircon U-Pb data for the Triassic granites in the Chifeng City, Inner Mongolia Autonomous Region in the north margin of the North China Craton

Sample	w_B (ppm)				Isotope ratio				T (Ma)			
	Pb	Th	U	Th/U	$^{207}Pb/^{235}U$±1σ		$^{206}Pb/^{238}U$±1σ		$^{207}Pb/^{235}U$±1σ		$^{206}Pb/^{238}U$±1σ	
D2711-1-01	6.76	157.88	131.29	1.20	0.28386	0.01513	0.03998	0.00065	254	12	253	4
D2711-1-02	5.96	124.37	120.59	1.03	0.28663	0.02161	0.04050	0.00068	256	17	256	4
D2711-1-03	4.35	81.53	91.89	0.89	0.28172	0.02290	0.03967	0.00076	252	18	251	5
D2711-1-04	3.84	53.86	82.86	0.65	0.29040	0.03007	0.04109	0.00074	259	24	260	5
D2711-1-05*	19.23	335.09	408.49	0.82	0.32711	0.01093	0.04096	0.00058	287	8	259	4
D2711-1-06	30.80	214.59	720.65	0.30	0.29460	0.01234	0.04070	0.00058	262	10	257	4
D2711-1-07	13.67	306.10	274.45	1.12	0.28109	0.01266	0.04000	0.00062	252	10	253	4
D2711-1-08	39.51	949.74	836.15	1.14	0.27722	0.00816	0.03838	0.00053	248	6	243	3
D2711-1-09	10.42	278.09	202.49	1.37	0.26947	0.01431	0.03830	0.00059	242	11	242	4
D2711-1-10	5.00	87.53	109.05	0.80	0.28737	0.02257	0.03877	0.00067	256	18	245	4
D2711-1-11	9.00	203.38	183.67	1.11	0.27530	0.01569	0.03900	0.00061	247	12	247	4
D2711-1-12	1.17	21.00	25.25	0.83	0.28325	0.04350	0.03979	0.00096	253	34	252	6
D2711-1-13	7.03	103.82	152.56	0.68	0.29972	0.02242	0.03971	0.00065	266	18	251	4
D2711-1-14	8.53	209.74	177.29	1.18	0.28684	0.01217	0.03993	0.00062	256	10	252	4
D2711-1-15	18.04	426.96	342.75	1.25	0.28738	0.01073	0.04033	0.00058	256	8	255	4
D2711-1-16	6.23	130.59	124.25	1.05	0.28507	0.02748	0.03986	0.00089	255	22	252	6
D2711-1-17*	7.48	108.07	171.04	0.63	0.30255	0.01928	0.03834	0.00064	268	15	243	4
D2711-1-18	14.45	264.30	296.88	0.89	0.28494	0.01021	0.04022	0.00058	255	8	254	4
D2711-1-19	3.69	54.32	79.73	0.68	0.28578	0.01738	0.04036	0.00075	255	14	255	5
D2711-1-20	11.11	249.39	224.69	1.11	0.27775	0.01390	0.03966	0.00062	249	11	251	4
D2711-1-21	3.75	59.31	80.42	0.74	0.29076	0.02525	0.04002	0.00073	259	20	253	5
D2711-1-22	2.92	47.62	64.53	0.74	0.27201	0.02150	0.03857	0.00072	244	17	244	4
D2711-1-23*	9.30	78.22	156.69	0.50	0.40001	0.01539	0.05438	0.00081	342	11	341	5
D2711-1-24	3.45	76.41	75.36	1.01	0.28464	0.03012	0.04031	0.00071	254	24	255	4
T101-01*	1.60	40.09	32.63	1.23	0.76864	0.08334	0.03955	0.00335	579	48	250	21
T101-02	1.68	36.40	31.21	1.17	0.87075	0.10003	0.04059	0.00174	636	54	257	11
T101-03	1.17	26.56	22.46	1.18	0.93123	0.07274	0.03952	0.00174	668	38	250	11
T101-04	1.68	35.56	32.41	1.10	0.77944	0.07417	0.04077	0.00158	585	42	258	10
T101-05	1.14	27.88	20.40	1.37	1.17313	0.11252	0.04075	0.00181	788	53	257	11
T101-06	1.66	38.92	31.71	1.23	0.70655	0.08072	0.03877	0.00203	543	48	245	13
T101-07	1.63	41.02	28.66	1.43	0.75538	0.12314	0.03837	0.00270	571	71	243	17
T101-08	1.20	28.85	22.62	1.28	0.81673	0.05816	0.04069	0.00195	606	33	257	12
T101-09	1.96	40.33	39.20	1.03	0.78539	0.14128	0.03773	0.00214	589	81	239	13
T101-10	1.38	30.51	25.51	1.20	0.94989	0.06963	0.04081	0.00176	678	36	258	11
T101-11	3.11	52.40	61.02	0.86	0.59640	0.04495	0.04096	0.00140	475	29	259	9
T101-12	1.33	24.54	22.23	1.10	1.57258	0.12535	0.04040	0.00172	959	50	255	11
T101-13	1.81	40.37	33.85	1.19	0.80155	0.06170	0.04027	0.00162	598	35	255	10
T101-14	3.80	72.13	80.63	0.89	0.43799	0.03252	0.03855	0.00103	369	23	244	6
T101-15	1.38	30.28	27.51	1.10	1.05524	0.09350	0.03803	0.00170	731	46	241	11
T101-16	1.99	55.79	42.40	1.32	0.90227	0.14203	0.03704	0.00166	653	76	234	10
T101-17	1.60	42.80	30.18	1.42	0.78529	0.07604	0.03816	0.00154	588	43	241	10
T101-18	1.25	36.30	24.72	1.47	0.99539	0.13652	0.03866	0.00172	701	70	244	11
T101-19	2.56	41.46	55.47	0.75	0.55569	0.04830	0.04032	0.00115	449	32	255	7
T101-20	1.33	37.23	26.14	1.42	0.69045	0.04380	0.04027	0.00138	533	26	254	9
PM210-6-1-01	6.68	121.42	139.37	0.87	0.27960	0.00981	0.03922	0.00053	250	8	248	3
PM210-6-1-02	13.86	193.56	307.78	0.63	0.29493	0.00796	0.03905	0.00050	262	6	247	3
PM210-6-1-03	9.51	162.88	202.45	0.80	0.27820	0.00797	0.03906	0.00051	249	6	247	3
PM210-6-1-04	11.54	164.39	255.88	0.64	0.27584	0.00707	0.03902	0.00050	247	6	247	3
PM210-6-1-05	13.54	190.34	297.67	0.64	0.27974	0.00767	0.03969	0.00052	250	6	251	3
PM210-6-1-06	11.94	137.74	265.29	0.52	0.28726	0.00876	0.04007	0.00052	256	7	253	3
PM210-6-1-07	11.64	235.89	240.32	0.98	0.27874	0.00795	0.03876	0.00051	250	6	245	3
PM210-6-1-08	14.43	223.00	319.14	0.70	0.27623	0.00743	0.03869	0.00050	248	6	245	3
PM210-6-1-09	7.66	152.37	152.86	1.00	0.28444	0.00938	0.03989	0.00054	254	7	252	3
PM210-6-1-10	14.43	229.12	315.56	0.73	0.28054	0.00792	0.03886	0.00050	251	6	246	3
PM210-6-1-11	14.00	275.67	289.43	0.95	0.27615	0.00728	0.03902	0.00051	248	6	247	3
PM210-6-1-12	25.56	389.62	559.64	0.70	0.28302	0.00661	0.03985	0.00050	253	5	252	3
PM210-6-1-13	9.04	116.98	199.98	0.58	0.28337	0.01088	0.04010	0.00055	253	9	253	3
PM210-6-1-14	8.93	115.62	202.74	0.57	0.27413	0.00860	0.03884	0.00052	246	7	246	3
PM210-6-1-15*	71.18	160.55	176.90	0.91	5.01581	0.10732	0.31872	0.00397	1822	18	1783	19
PM210-6-1-16	10.32	197.46	216.78	0.91	0.27663	0.00952	0.03883	0.00051	248	8	246	3
PM210-6-1-17	12.61	224.10	273.11	0.82	0.27211	0.00787	0.03872	0.00051	244	6	245	3
PM210-6-1-18	10.28	180.69	223.14	0.81	0.29942	0.00999	0.03893	0.00051	266	8	246	3
PM210-6-1-19	12.03	180.28	262.90	0.69	0.27786	0.00871	0.03952	0.00053	249	7	250	3
PM210-6-1-20	12.78	231.74	269.35	0.86	0.27635	0.00817	0.03885	0.00051	248	6	246	3
PM210-6-1-21	16.77	251.43	373.32	0.67	0.28182	0.00739	0.03883	0.00050	252	6	246	3
PM210-6-1-22	8.57	140.42	187.00	0.75	0.29004	0.01119	0.03854	0.00054	259	9	244	3
PM210-6-1-23	5.31	94.28	115.41	0.82	0.27754	0.00978	0.03859	0.00054	249	8	244	3
PM210-6-1-24	11.51	212.30	244.43	0.87	0.28534	0.00889	0.03899	0.00052	255	7	247	3
PM210-6-1-25	17.33	203.65	401.79	0.51	0.27998	0.00772	0.03935	0.00051	251	6	249	3
PM101-7-2-01	8.61	142.04	186.69	0.76	0.26933	0.04082	0.03772	0.00163	242	33	239	10
PM101-7-2-02*	24.08	374.97	519.92	0.72	0.21816	0.02474	0.04019	0.00096	200	21	254	6

Continued Table 1

Sample	w_B (ppm)			Th/U	Isotope ratio				T (Ma)			
	Pb	Th	U		$^{207}Pb/^{235}U±1σ$		$^{206}Pb/^{238}U±1σ$		$^{207}Pb/^{235}U±1σ$		$^{206}Pb/^{238}U±1σ$	
PM101-7-2-03*	11.86	156.03	299.89	0.52	0.19816	0.02161	0.03504	0.00147	184	18	222	9
PM101-7-2-04	11.32	211.21	231.44	0.91	0.28954	0.03642	0.03791	0.00117	258	29	240	7
PM101-7-2-05	14.22	210.06	312.19	0.67	0.27320	0.01495	0.03868	0.00114	245	12	245	7
PM101-7-2-06	23.17	341.93	530.49	0.64	0.28098	0.02862	0.03908	0.00093	251	23	247	6
PM101-7-2-07	22.56	320.12	513.55	0.62	0.28251	0.01330	0.03837	0.00068	253	11	243	4
PM101-7-2-08	17.14	269.04	403.56	0.67	0.27131	0.01794	0.03754	0.00102	244	14	238	6
PM101-7-2-09	11.33	185.81	254.53	0.73	0.27872	0.02183	0.03811	0.00103	250	17	241	6
PM101-7-2-10	27.44	457.68	640.34	0.71	0.28238	0.01212	0.03822	0.00063	253	10	242	4
PM101-7-2-11	14.73	192.81	362.72	0.53	0.28310	0.01703	0.03783	0.00081	253	13	239	5
PM101-7-2-12	24.60	369.87	570.75	0.65	0.27892	0.01159	0.03920	0.00071	250	9	248	4
PM101-7-2-13	17.43	289.43	410.90	0.70	0.27770	0.02168	0.03785	0.00055	249	17	239	3
PM101-7-2-14	19.73	260.21	469.52	0.55	0.28135	0.01223	0.03966	0.00069	252	10	251	4
PM101-7-2-15	5.54	104.16	131.16	0.79	0.29169	0.01864	0.03802	0.00101	260	15	241	6
PM101-7-2-16	24.98	327.04	573.08	0.57	0.29370	0.03144	0.04029	0.00122	261	25	255	8
PM101-7-2-17	20.77	326.66	475.35	0.69	0.27771	0.01085	0.03901	0.00065	249	9	247	4
PM101-7-2-18	16.62	218.85	398.18	0.55	0.28638	0.01550	0.03925	0.00083	256	12	248	5
PM101-7-2-19	37.62	511.76	926.91	0.55	0.27092	0.01178	0.03821	0.00067	243	9	242	4
PM101-7-2-20	22.00	278.30	513.17	0.54	0.30168	0.01318	0.03927	0.00065	268	10	248	4
D3493-1-01	11.94	231.73	245.25	0.94	0.27272	0.01044	0.03873	0.00049	245	8	245	3
D3493-1-02*	19.48	283.98	468.93	0.61	0.27809	0.00875	0.03593	0.00045	249	7	228	3
D3493-1-03	8.49	104.00	195.07	0.53	0.27618	0.01361	0.03783	0.00052	248	11	239	3
D3493-1-04*	8.02	130.86	191.91	0.68	0.31441	0.01730	0.03355	0.00053	278	13	213	3
D3493-1-05	11.60	265.66	227.95	1.17	0.26734	0.01207	0.03898	0.00049	241	10	247	3
D3493-1-06	4.93	81.78	106.53	0.77	0.27761	0.02109	0.03842	0.00055	249	17	243	3
D3493-1-07	17.00	248.36	373.45	0.67	0.27450	0.00909	0.03885	0.00049	246	7	246	3
D3493-1-08	13.98	313.98	274.52	1.14	0.27296	0.01269	0.03876	0.00049	245	10	245	3
D3493-1-09	11.19	224.95	228.39	0.98	0.27606	0.01086	0.03859	0.00050	248	9	244	3
D3493-1-10	6.71	117.22	143.10	0.82	0.27305	0.01204	0.03853	0.00053	245	10	244	3
D3493-1-11	8.28	121.94	183.68	0.66	0.26613	0.01052	0.03855	0.00052	240	8	244	3
D3493-1-12*	115	1794	2472	0.73	0.38384	0.00867	0.03881	0.00046	330	6	245	3
D3493-1-13	49.54	642.61	1060	0.61	0.28433	0.01255	0.03888	0.00049	254	10	246	3
D3493-1-14	9.06	202.82	181.02	1.12	0.27813	0.01538	0.03835	0.00053	249	12	243	3
D3493-1-15	6.29	118.68	131.77	0.90	0.27526	0.01418	0.03855	0.00055	247	11	244	3
D3493-1-16	17.98	531.30	331.91	1.60	0.27059	0.01026	0.03812	0.00048	243	8	241	3
D3493-1-17	13.20	206.55	292.19	0.71	0.26659	0.00927	0.03847	0.00049	240	7	243	3
D3493-1-18	12.83	225.62	284.14	0.79	0.26369	0.01221	0.03726	0.00052	238	10	236	3
D3493-1-19	7.42	260.54	125.38	2.08	0.27440	0.02007	0.03817	0.00057	246	16	241	4
D3493-1-20	11.04	168.94	244.30	0.69	0.26922	0.01089	0.03858	0.00050	242	9	244	3
D3493-1-21	10.38	205.05	221.10	0.93	0.27162	0.01114	0.03840	0.00051	244	9	243	3
D3493-1-22	41.81	620.47	938.91	0.66	0.26118	0.00834	0.03836	0.00049	236	7	243	3
D3493-1-23*	14.82	145.77	253.32	0.58	0.20793	0.02402	0.03275	0.00046	192	20	208	3
D3493-1-24	12.56	137.42	292.39	0.47	0.26743	0.02054	0.03875	0.00072	241	16	245	4
D3493-1-25	5.33	93.98	115.00	0.82	0.27543	0.02871	0.03854	0.00061	247	23	244	4
14CH14-01	106	379	1876	0.20	0.25797	0.00895	0.03716	0.00039	233	7	235	2
14CH14-02	80	388	977	0.39	0.27184	0.01235	0.03673	0.00046	244	10	233	3
14CH14-03*	84	352	977	0.35	0.30114	0.01349	0.03818	0.00046	267	11	242	3
14CH14-04*	1125	665	2043	0.30	4.22415	0.12125	0.27072	0.00571	1679	24	1544	29
14CH14-05*	91	458	882	0.50	0.27534	0.01230	0.03966	0.00059	247	10	251	4
14CH14-06*	80	365	1033	0.34	0.28399	0.01115	0.03757	0.00047	254	9	238	3
14CH14-07	90	417	1201	0.34	0.26498	0.01061	0.03681	0.00043	239	9	233	3
14CH14-08	119	531	1902	0.27	0.25283	0.00850	0.03563	0.00036	229	7	226	2
14CH14-09	95	422	1280	0.30	0.27103	0.01018	0.03667	0.00041	244	8	232	3
14CH14-10	211	1118	2318	0.46	0.25408	0.00750	0.03527	0.00032	230	6	223	2
14CH14-11	119	569	1349	0.38	0.27113	0.00921	0.03636	0.00041	244	7	230	3
14CH14-12*	206	1103	2078	0.51	0.26597	0.00821	0.03470	0.00038	239	7	220	2
14CH14-13	108	510	1314	0.37	0.27034	0.00999	0.03694	0.00042	243	8	234	3
14CH14-14	174	823	2133	0.37	0.25864	0.00861	0.03670	0.00036	234	7	232	2
14CH14-15	77	363	1005	0.35	0.25839	0.01142	0.03566	0.00046	233	9	226	3
14CH14-16*	46	194	398	0.44	0.35626	0.02154	0.03578	0.00061	309	16	227	4
14CH14-17*	75	369	682	0.52	0.27834	0.01383	0.03513	0.00047	249	11	223	3
14CH14-18*	67	301	933	0.30	0.25106	0.01062	0.03855	0.00051	227	9	244	3
14CH14-19	84	413	962	0.41	0.26357	0.01151	0.03643	0.00043	238	9	231	3
14CH14-20	64	363	596	0.56	0.26065	0.01421	0.03688	0.00070	235	11	233	4
T409-01*	124	512	247	2.07	0.66196	0.03268	0.04843	0.00115	516	20	305	7
T409-02*	392	408	218	1.87	1.40546	0.03531	0.04860	0.00074	891	15	306	5
T409-03*	1139	443	452	0.98	1.69171	0.06081	0.04663	0.00117	1005	23	294	7
T409-04*	215	1974	765	2.58	0.47380	0.05099	0.04657	0.00156	394	35	293	10
T409-05*	883	3140	533	5.90	1.50018	0.04418	0.04706	0.00066	930	18	296	4
T409-06*	731	1780	437	4.07	1.27712	0.06097	0.04606	0.00154	836	27	290	10
T409-07*	1271	265	183	1.45	3.44493	0.08164	0.04786	0.00066	1515	19	301	4
T409-08*	304	1279	339	3.77	0.90627	0.04242	0.04751	0.00080	655	23	299	5
T409-09*	421	1069	358	2.99	1.26014	0.03984	0.04799	0.00058	828	18	302	4

Continued Table 1

Sample	w_B (ppm)				Isotope ratio				T (Ma)			
	Pb	Th	U	Th/U	$^{207}Pb/^{235}U±1\sigma$		$^{206}Pb/^{238}U±1\sigma$		$^{207}Pb/^{235}U±1\sigma$		$^{206}Pb/^{238}U±1\sigma$	
T409-10*	189	985	622	1.58	0.41912	0.02972	0.03752	0.00115	355	21	237	7
T409-11*	452	2763	611	4.53	1.31036	0.04053	0.03611	0.00078	850	18	229	5
T409-12	57	994	329	3.02	0.26577	0.01888	0.03738	0.00092	233	15	232	6
T409-13*	132	683	624	1.09	0.59580	0.02117	0.03832	0.00093	475	13	242	6
T409-14*	294	1019	363	2.81	1.12912	0.04248	0.03702	0.00119	767	20	234	7
T409-15*	431	1369	337	4.06	1.30177	0.04202	0.03659	0.00061	847	19	232	4
T409-16	53	633	421	1.50	0.25834	0.01989	0.03668	0.00078	233	16	232	5
T409-17*	205	813	332	2.45	0.64869	0.02308	0.03639	0.00059	508	14	230	4
T409-18*	632	1414	295	4.80	1.87100	0.04989	0.03573	0.00048	1071	18	226	3
T409-19*	203	689	239	2.89	0.51140	0.01619	0.03713	0.00047	419	11	235	3

*Representing the abandoned points when calculating weighted average age because of discordance.

pluton. Twenty U-Pb analyses were obtained, twelve of which give a range of $^{206}Pb/^{238}U$ ages between 235 and 226 Ma and cluster in a single group on or near the concordia. Their weighted mean $^{206}Pb/^{238}U$ age is 230±2 Ma (MSDW=2.5; n=12) (Fig. 5f), which is interpreted to represent the crystallization timing of the granodiorite. This age is consistent (within error) with the age of 227±1 Ma obtained by Zhang (2013).

Sample T409 is a monzogranite from the Bajiazi pluton. Nineteen U-Pb analyses were obtained, only two of which are distributed on/near the concordia, possibly because of the high contents of common lead. The weighted mean $^{206}Pb/^{238}U$ age is 232±4 Ma (MSDW=0.78; n=2) (Figs. 5g, 5h). This age is interpreted to be the crystallization age of the monzogranite and is consistent with the age (233 Ma) obtained by Song et al. (2010).

4.1.4 Zircon U-Pb age groups

Based on the new ages and previous age data (Duan et al., 2014; Zhang, 2013; Song et al., 2010), Triassic granites in the Chifeng area can be divided into three main groups. The syenogranites (D2711-1, T101, and PM210-6-1) with ages of 250–248 Ma belong to the Early Triassic, the granodiorites (PM107-7-2 and D3493-1) with ages of 244–243 Ma belong to the Middle Triassic, and the granodiorite (14CH14) and monzogranite (T409) with ages of 230 Ma and 232 Ma, respectively, belong to the early Late Triassic.

4.2 Major- and trace-element geochemistry

A total of 27 granitic samples, including syenogranite, granodiorite, and monzogranite, were analyzed for major- and trace-element compositions. The results are listed in Table 2.

4.2.1 Early Triassic syenogranite

The syenogranite samples all contain high contents of SiO_2 (73.41–76.65 wt%), K_2O (3.77–5.11 wt%), and total Na_2O+K_2O (7.92–9.13 wt%), and plot within the high-K calc-alkaline fields in a K_2O vs. SiO_2 diagram (Fig. 6a; Peccerillo and Taylor, 1976). The samples also contain low contents of Al_2O_3 (11.54–13.50 wt%), TiO_2 (0.07–0.18 wt%), MnO (0.02–0.07 wt%), MgO (0.10–0.19 wt%), and P_2O_5 (0.01–0.04 wt%), with total Fe_2O_3 (TFe_2O_3) of 1.32–2.99 wt%. Their A/CNK [molar $Al_2O_3/(Na_2O+K_2O+CaO)$] values range from 0.96 to 1.06, indicating a metaluminous to weakly peraluminous nature, as shown in an A/NK vs. A/CNK diagram (Fig. 6b;

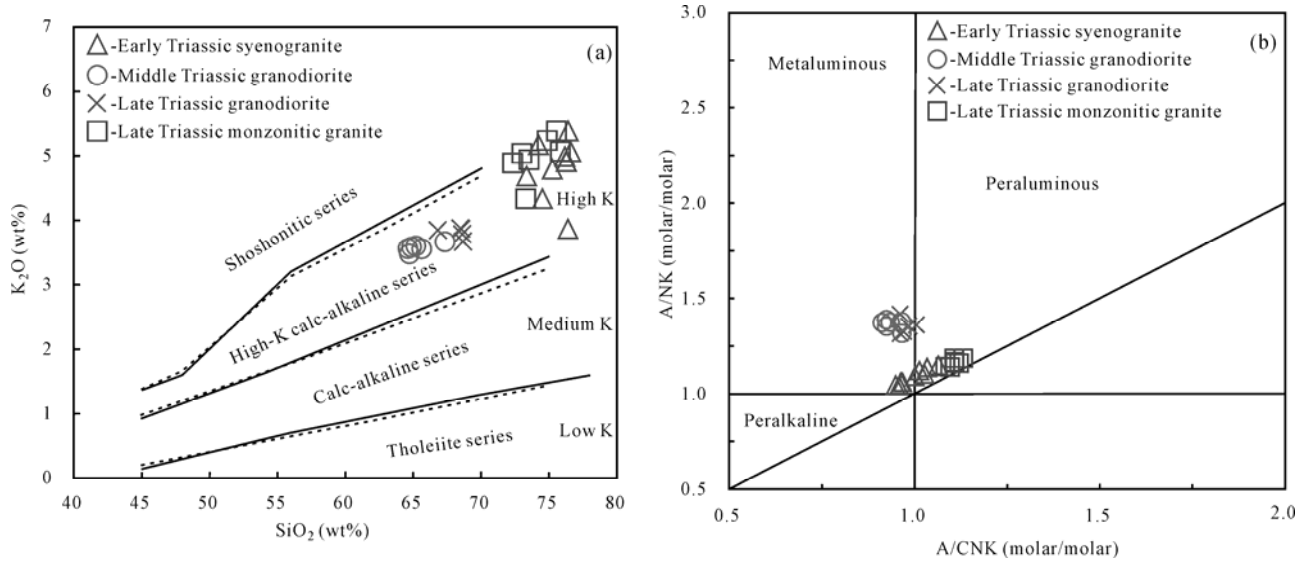

Fig. 6. (a) K_2O versus SiO_2 diagram for intrusive rocks. Normalization values are from Le Maitre (1984) and Rickwood (1989); (b) A/NK (molar/molar) versus A/CNK (molar/molar) diagram for these rocks. Normalization values are from Le Maitre (1984) and Rickwood (1989).

Table 2 Major (wt%) and trace (ppm) elements data of Triassic granites in the Chifeng City, Inner Mongolia Autonomous Region in the north margin of the North China Craton

Sample	D2711-1	D2711-2	PM205-2-2	PM205-4-1	PM205-10-1	PM210-2-1	PM210-6-1	PM210-8-2	PM210-8-3
Lithology	Syenogrinite					Syenogrinite			
Pluton	Xiaxinjing					Daluobogou			
Era	Early Triassic								
SiO_2	74.28	75.48	74.51	76.56	73.41	76.21	76.37	76.65	76.44
TiO_2	0.18	0.09	0.12	0.1	0.15	0.07	0.08	0.08	0.08
Al_2O_3	13.09	12.54	13.16	12.33	13.5	12.36	12.33	11.96	11.54
TFe_2O_3	2.04	1.78	2.08	1.87	2.99	1.45	1.32	1.83	2.2
FeO	0.76	0.9	0.88	0.86	1.6	0.79	0.61	0.97	1.4
MnO	0.06	0.04	0.04	0.04	0.07	0.02	0.02	0.03	0.03
MgO	0.13	0.18	0.19	0.17	0.09	0.1	0.1	0.1	0.11
CaO	0.39	0.49	0.58	0.4	0.51	0.57	0.53	0.5	0.52
Na_2O	4.02	3.89	4.31	4.15	4.12	3.88	3.89	3.62	3.23
K_2O	5.11	4.76	4.28	3.77	4.63	4.94	4.93	5.09	5.36
P_2O_5	0.03	0.01	0.03	0.02	0.04	0.01	0.01	0.01	0.01
LOI	0.47	0.5	0.47	0.4	0.3	0.24	0.27	0.04	0.34
Total	100.5	100.6	100.6	100.6	101.4	100.6	100.4	100.8	101.2
Na_2O+K_2O	9.13	8.65	8.59	7.92	8.75	8.82	8.82	8.72	8.59
Na_2O/K_2O	0.79	0.82	1.01	1.1	0.89	0.79	0.79	0.71	0.6
A/NK	1.08	1.09	1.12	1.13	1.15	1.05	1.05	1.04	1.04
A/CNK	1.02	1.01	1.03	1.06	1.06	0.97	0.97	0.97	0.96
SI	1.09	1.57	1.65	1.57	0.64	0.93	0.93	0.83	0.87
AR	3.96	3.97	4.33	4.3	3.85	4.01	4.06	3.78	3.3
σ43	2.66	2.3	2.34	1.87	2.53	2.34	2.33	2.26	2.21
σ25	1.69	1.48	1.49	1.22	1.57	1.52	1.51	1.47	1.43
R1	2250	2458	2349	2664	2198	2474	2498	2533	2574
R2	305	307	330	292	321	307	303	291	285
$Mg^{\#}$	0.1	0.12	0.13	0.12	0.03	0.08	0.1	0.06	0.05
La	40.33	23.8	28.59	23.87	34.15	23.43	24.97	33.78	22.01
Ce	85.28	56.17	63.43	49.73	62.69	53.1	64.81	76.88	59.66
Pr	8.43	5.08	5.56	5.83	6.77	7.46	7.74	9.28	6.25
Nd	28.24	16.75	18.06	22.94	22.11	28.93	29.73	33.36	22.67
Sm	4.25	3.06	2.92	4.98	3.72	7.2	6.79	6.05	4.6
Eu	0.76	0.75	0.68	0.97	0.59	0.17	0.16	0.14	0.19
Gd	3.55	2.19	2.51	4.33	3.06	3.96	4.06	4.06	3.09
Tb	0.43	0.33	0.34	0.78	0.43	0.77	0.76	0.57	0.56
Dy	2.38	2.01	1.89	4.94	2.43	5.21	5.41	3.06	3.78
Ho	0.51	0.42	0.38	1.05	0.65	0.94	1.07	0.58	0.75
Er	1.51	1.06	1.14	2.77	1.47	2.16	2.64	1.47	1.85
Tm	0.34	0.2	0.21	0.48	0.24	0.39	0.49	0.24	0.33
Yb	2.57	1.36	1.42	3.07	1.52	2.44	3.08	1.56	2.11
Lu	0.46	0.21	0.22	0.46	0.23	0.37	0.46	0.23	0.31
Y	16.05	11.6	11.66	30.19	15.89	24.13	28.77	14.06	19.6
ΣREE	179	113	127	126	140	136	152	171	128
LREE	167.3	105.6	119.2	108.3	130	120.3	134.2	159.4	115.3
HREE	11.74	7.78	8.1	17.86	10.03	16.24	17.97	11.76	12.79
LREE/HREE	14.25	13.58	14.72	6.06	12.97	7.41	7.47	13.56	9.02
La_N/Yb_N	11.25	12.56	14.47	5.58	16.16	6.88	5.81	15.53	7.47
δEu	0.58	0.84	0.75	0.62	0.52	0.09	0.09	0.08	0.14
δCe	1.08	1.19	1.16	1	0.95	0.98	1.13	1.05	1.23
Sc	5.59	5.27	4.34	3.8	3.49	5.34	5.26	5.24	4.32
Co	2.24	2.18	1.03	0.39	0.75	2.94	2.83	0.72	2.23
Ni	1.69	3.58	7.32	7.25	7.95	2.88	1.82	2.68	2.57
Be	3.77	2.38	3.4	2.55	2.01	3.03	3.05	2.81	2.05
Rb	175	87	128	120	133	193	195	142	152
Sr	84.54	42.36	77.55	62.61	108.3	24.69	28.26	19.12	27.84
Ba	339	506	572	429	656	72	103	60	86
Zr	134	82.66	104	106	121	120	135	126	116
Nb	18.89	12.11	16.35	20.8	14.67	30.95	29.38	13.12	14.12
Hf	5.8	3.08	3.19	3.4	3.8	5.82	6.65	5.34	4.85
Ta	1.62	1.45	2.11	2.04	1.8	2.3	2.46	0.96	1.91
Th	6.63	10.91	10.64	11.68	5.18	11.01	7.85	14.3	12.74
U	2.17	1.01	1	1.39	1.97	2.21	2.37	1.43	1.63
Sr/Y	5.27	3.65	6.65	2.07	6.82	1.02	0.98	1.36	1.42
Zr+Nb+Ce+Y	254	162	195	207	214	228	258	230	210

Continued Table 2

Sample	PM101-5-1	PM101-7-1	PM101-7-2	PM101-7-3	PM101-7-4	PM101-7-5	PM403-3-1	PM403-5-1	PM403-7-1
Lithology	Granodiorite						Monzogranite		
Pluton	Mengguyingzi						Bajiazi		
Era	Middle Triassic						Late Triassic		
SiO_2	65.17	65.74	64.7	65.29	67.41	64.68	72.56	75.04	75.81
TiO_2	0.65	0.69	0.76	0.69	0.54	0.77	0.36	0.17	0.16
Al_2O_3	16.07	15.66	16.08	15.93	15.48	15.89	14.5	13.14	13.16
TFe_2O_3	4.27	4.21	4.35	4.15	3.58	4.48	1.41	1.56	0.75
FeO	3.01	2.65	3.01	2.57	2.29	2.88	0.54	0.54	0.36
MnO	0.06	0.07	0.07	0.06	0.07	0.07	0.01	0.02	0.01
MgO	1.77	1.73	1.92	1.79	1.45	2	0.11	0.07	0.01
CaO	2.97	2.64	3.15	2.97	2.3	3.17	0.35	0.27	0.25
Na_2O	4.73	4.59	4.77	4.76	4.76	4.69	4.46	3.23	3.38
K_2O	3.61	3.52	3.45	3.62	3.66	3.57	4.94	5.46	5.4
P_2O_5	0.21	0.22	0.24	0.22	0.18	0.25	0.03	0.02	0.01
LOI	0.27	0.76	0.31	0.32	0.4	0.2	1	0.82	0.88
Total	102.8	102.4	102.8	102.3	102.1	102.6	100.2	100.3	100.1
Na_2O+K_2O	8.34	8.12	8.23	8.38	8.42	8.26	9.4	8.69	8.78
Na_2O/K_2O	1.31	1.3	1.38	1.32	1.3	1.31	0.9	0.59	0.63
A/NK	1.37	1.38	1.39	1.36	1.31	1.37	1.14	1.17	1.15
A/CNK	0.94	0.97	0.93	0.93	0.97	0.92	1.1	1.12	1.11
SI	10.23	10.44	11.06	10.66	9.25	11.43	0.97	0.64	0.07
AR	2.56	2.59	2.5	2.59	2.8	2.53	4.02	2.85	3.03
σ43	3.22	2.94	3.2	3.21	2.94	3.22	2.98	2.35	2.34
σ25	1.72	1.61	1.69	1.73	1.66	1.71	1.87	1.51	1.52
R1	1570	1700	1558	1590	1750	1560	2048	2528	2571
R2	704	665	730	706	612	733	330	292	287
$Mg^{\#}$	0.28	0.3	0.3	0.32	0.3	0.32	0.12	0.08	0.01
La	43.16	43.17	50.25	46.49	38.11	50.69	52.78	29.15	29.57
Ce	95.95	104.1	115.1	106.1	84.56	114.2	102.4	49.53	51.94
Pr	12.56	13.42	14.84	13.64	10.13	14.82	11.01	5.08	4.67
Nd	46.92	47.83	56.23	51.48	35.49	55.92	38.56	16.41	14.23
Sm	7.79	7.69	9.69	8.76	5.98	9.41	6.09	2.45	1.84
Eu	1.63	1.46	2.11	1.88	1.45	2.03	1.18	0.69	0.54
Gd	6.06	6.46	7.31	6.57	4.63	7.14	4.53	1.93	1.53
Tb	0.89	0.89	1.07	0.98	0.68	1.06	0.64	0.24	0.18
Dy	4.326	4.411	5.188	4.643	3.24	5.101	3.09	1.18	0.82
Ho	0.79	0.81	0.92	0.84	0.6	0.94	0.54	0.2	0.14
Er	2.09	2.2	2.46	2.28	1.97	2.46	1.33	0.53	0.4
Tm	0.34	0.36	0.4	0.38	0.29	0.39	0.18	0.08	0.05
Yb	2.3	2.69	2.7	2.57	1.96	2.76	1.14	0.56	0.4
Lu	0.28	0.32	0.32	0.32	0.26	0.32	0.16	0.09	0.07
Y	24.98	25.34	28.02	26.86	19.54	29.32	14.23	5.26	3.73
ΣREE	225	235	268	246	189	267	223	108	106
LREE	208	217	248	228	175	247	212	103	102
HREE	17.09	18.15	20.37	18.57	13.63	20.18	11.61	4.81	3.59
LREE/HREE	12.17	11.99	12.19	12.3	12.89	12.25	18.27	21.49	28.64
La_N/Yb_N	13.45	11.5	13.36	12.97	13.97	13.18	33.33	37.61	53.43
δEu	0.7	0.62	0.74	0.73	0.81	0.73	0.66	0.93	0.96
δCe	1	1.05	1.02	1.02	1.03	1.01	0.99	0.92	0.98
Sc	6.97	7.53	7.75	7.28	6.33	7.83	1.72	1.24	1.2
Co	9.58	8.75	9.43	10.23	7.45	10.39	0.53	1.74	0.24
Ni	14.36	16.2	16.9	15.36	12.2	15.58	1.13	2.3	0.01
Be	3.16	3.13	3.37	3.17	3.15	3.22	1.31	1.5	1.08
Rb	109	129	106	106	118	109	115	125	122
Sr	671	507	661	653	558	656	365	234	230
Ba	784	641	733	768	712	789	942	552	517
Zr	232	224	222	197	170	244	174	131	124
Nb	18.84	23.91	17.94	18.89	17.3	19.14	14.39	6.2	6.59
Hf	6.53	6.83	8	6.43	6.53	7.44	4.4	3.37	3.82
Ta	1.42	2.26	2.29	2.1	1.83	2.12	0.96	0.51	0.38
Th	16.69	19.08	22.46	19.51	14.21	24.86	9.43	7.89	5.6
U	2.78	2.84	3.48	3.03	3.19	3.72	1.03	0.69	0.6
Sr/Y	26.88	20.05	23.62	24.33	28.56	22.39	25.68	44.6	61.85
Zr+Nb+Ce+Y	372	378	384	349	291	406	305	192	186

Continued Table 2

Sample	PM403-7-2	PM403-7-3	PM403-7-4	PM403-7-5	14CH13	14CH14	14CH15	14CH16	14CH17
Lithology	Monzogranite				Granodiorite				
Pluton	Bajiazi				Ailingou				
Era	Late Triassic								
SiO_2	74.91	73.56	73.36	73.03	68.76	68.67	68.98	68.54	66.79
TiO_2	0.19	0.35	0.33	0.35	0.5	0.54	0.51	0.54	0.73
Al_2O_3	12.91	14.01	14.24	14.8	14.95	14.8	14.58	14.73	15.18
TFe_2O_3	1.17	0.91	1.6	1.25	3.56	3.82	3.65	3.68	4.38
FeO	0.67	0.31	0.45	0.49	1.63	2.28	2.53	2.88	3.25
MnO	0.01	0	0.01	0.01	0.06	0.07	0.06	0.07	0.07
MgO	0.8	0.27	0.09	0.03	0.89	0.99	0.97	0.94	1.4
CaO	0.44	0.37	0.33	0.29	2.13	2.2	2.21	2.31	2.92
Na_2O	3.12	4	4.34	4.01	4.17	4.2	4.05	4.22	3.92
K_2O	5.32	4.99	4.4	5.05	3.83	3.71	4	3.91	3.85
P_2O_5	0.02	0.03	0.05	0.04	0.16	0.15	0.16	0.15	0.18
LOI	0.91	0.99	1.05	0.95	0.89	0.75	0.74	0.92	0.57
Total	100.4	99.79	100.2	100.2	99.9	99.9	99.9	100	100
Na_2O+K_2O	8.44	9	8.74	9.06	8	7.91	8.05	8.13	7.77
Na_2O/K_2O	0.59	0.8	0.99	0.79	1.09	1.13	1.01	1.08	1.02
A/NK	1.19	1.17	1.2	1.23	1.36	1.36	1.33	1.32	1.43
A/CNK	1.1	1.11	1.14	1.18	1.01	0.99	0.97	0.96	0.95
SI	7.24	2.55	0.8	0.31	6.4	6.66	6.39	6.03	8.39
AR	2.75	3.51	3.94	3.26	2.76	2.74	2.84	2.82	2.5
σ43	2.23	2.64	2.51	2.72	2.49	2.46	2.52	2.62	2.59
σ25	1.43	1.68	1.59	1.71	1.46	1.42	1.46	1.51	1.43
R1	2594	2297	2273	2223	2046	2015	2014	1930	1889
R2	341	332	322	325	563	567	561	572	663
$Mg^{\#}$	0.44	0.36	0.11	0.04	0.27	0.22	0.2	0.18	0.22
La	38.23	48.74	56.19	50.01	49.7	41.2	36.3	40.1	28.4
Ce	66.09	97.75	108.5	99.82	94.4	79.6	74.4	84.1	60.1
Pr	5.83	10.12	11.66	10.48	11.4	9.37	8.71	9.55	7.39
Nd	17.21	35.18	40.64	36.18	42.5	34.6	33	35.7	29.1
Sm	2.09	5.43	6.44	5.54	8.14	6.38	6.61	6.96	5.65
Eu	0.57	1.13	1.25	1.08	1.26	1	1.05	1.05	1.16
Gd	1.78	3.96	4.98	4.08	8.51	6.75	6.58	7.14	5.72
Tb	0.19	0.53	0.7	0.53	1.17	0.9	1.02	1.04	0.79
Dy	0.79	2.59	3.61	2.6	6.03	4.89	5.37	5.73	4.3
Ho	0.15	0.46	0.62	0.51	1.24	1.05	1.16	1.16	0.9
Er	0.4	1.13	1.6	1.18	3.46	2.83	2.92	3.16	2.37
Tm	0.06	0.17	0.21	0.18	0.51	0.42	0.42	0.43	0.38
Yb	0.45	1.09	1.35	1.1	3.5	2.78	2.71	3.04	2.29
Lu	0.07	0.16	0.18	0.15	0.48	0.36	0.37	0.4	0.3
Y	4.51	12.05	16.79	15.09	32.6	25.4	27.3	28.3	21.3
ΣREE	133	208	237	213	232	192	180	199	148
LREE	130	198	224	203	207	172	160	177	131
HREE	3.88	10.08	13.25	10.33	24.9	19.98	20.55	22.1	17.05
LREE/HREE	33.55	19.67	16.95	19.66	8.33	8.61	7.79	8.03	7.73
La_N/Yb_N	60.67	31.94	29.92	32.55	10.19	10.63	9.61	9.46	8.9
δEu	0.89	0.71	0.65	0.67	0.46	0.46	0.48	0.45	0.62
δCe	0.97	1.02	0.99	1.02	0.94	0.95	0.99	1.02	0.99
Sc	1.37	2.12	2.07	2.23	7.69	6.72	6.89	6.64	6.95
Co	0.44	0.34	2.33	0.79	6.64	6.08	5.4	4.94	7.99
Ni	1.2	0.48	0.98	0.73	5.59	4.45	4.7	4.41	6.5
Be	1.13	1.17	1.37	1.25	3.81	2.89	2.71	2.65	1.75
Rb	121	112	109	118	137	113	120	109	98
Sr	228	359	336	365	312	240	253	239	314
Ba	523	856	891	905	676	499	596	532	645
Zr	153	184	164	187	330	277	245	287	224
Nb	6.97	14.7	13.98	15.31	26.6	22.8	24.1	24.7	20.8
Hf	3.62	5.51	4.3	4.93	8.38	7.12	6.36	7.43	5.98
Ta	0.39	1.02	1.1	0.9	2.13	1.84	1.81	1.87	2.02
Th	5.82	7.55	8.81	7	15.6	15.3	12.7	14.9	11.5
U	0.6	0.8	1.14	0.96	2.36	2.09	2.15	2.23	2.14
Sr/Y	50.62	29.87	20.07	24.22	9.57	9.45	9.27	8.45	14.74
Zr+Nb+Ce+Y	231	308	303	317	483	404	370	424	326

Maniar and Piccoli, 1989).

Total REE (ΣREE) contents of the syenogranite samples are 113–179 ppm, close to the continental crust average value of 154.7 ppm. The chondrite-normalized REE patterns exhibit enrichment of light REE (LREEs) relative to heavy REEs (HREEs), with ΣLREE/ΣHREE ratios and $(La/Yb)_N$ ratios of 7.41–14.72 and 5.58–16.16, respectively (Fig. 7a; Sun and McDonough, 1989). The samples exhibit negative Eu anomalies (Eu/Eu*=0.08–0.84). They also display enrichment in high-field-strength elements (HFSEs) and depletion in large-ion lithophile elements (LILEs), with negative Ba, K, Sr, P, and Ti anomalies, and positive Nb, Ta, Zr, and Hf anomalies (Fig. 7b; Sun and McDonough, 1989).

4.2.2 Middle Triassic granodiorite

SiO_2 contents of the Middle Triassic granodiorites vary within a narrow range from 64.68 to 65.74 wt%. The samples contain relatively high contents of K_2O (3.45–3.66 wt%) and are classified as high-K calc-alkaline series in a K_2O vs. SiO_2 diagram (Fig. 6a; Peccerillo and Taylor, 1976). These samples also have contents of Al_2O_3=15.48–16.08 wt%, TFe_2O_3=3.58–4.48 wt%, CaO=2.30–3.15 wt%, MnO=0.06–0.07 wt%, and P_2O_5=0.18–0.25 wt%. The A/CNK ratios range from 0.92 to 0.97, indicative of metaluminous granites (Fig. 6b; Maniar and Piccoli,

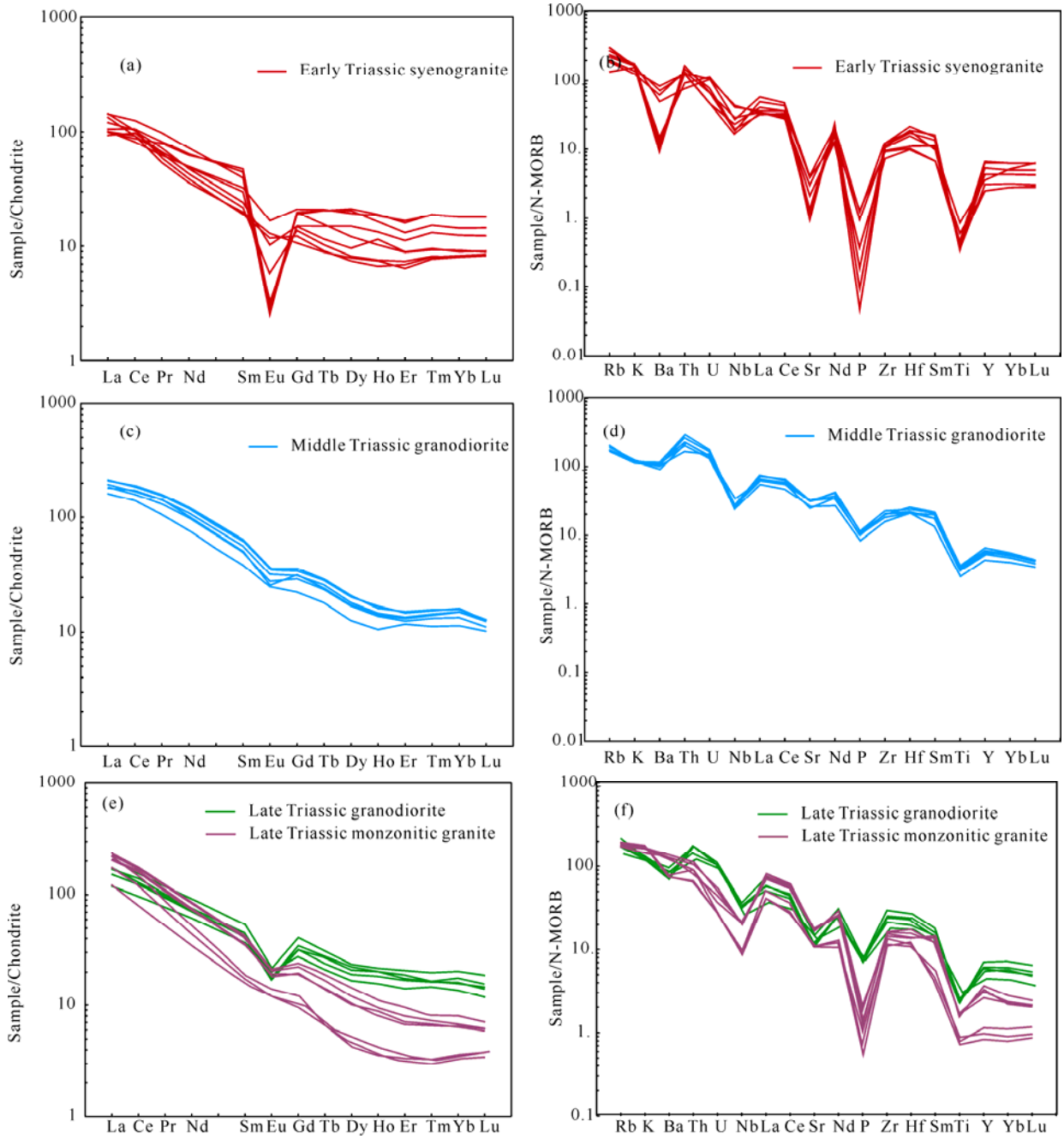

Fig. 7. (a, c, e) Chondrite-normalized rare earth element patterns and (b, d, f) primitive mantle normalized trace element spider diagram for these Triassic granitic rocks. The values of chondrite and primitive mantle are from Sun and McDonough (1989).

1989).

ΣREE contents of the granodiorites are 189–267 ppm, higher than the average value of continental crust (154.7 ppm). The samples are enriched in LREEs relative to HREEs in a chondrite-normalized REE diagram (Fig. 7c; Sun and McDonough, 1989), with ΣLREE/ΣHREE ratios and $(La/Yb)_N$ ratios of 11.99–12.89 and 11.50–13.97, respectively, and exhibit moderate negative Eu anomalies (Eu/Eu*=0.62–0.81). The granodiorites are enriched in LILEs (e.g., Rb, Ba, Th, U, and K) and depleted in HFSEs (e.g., Nb, Sr, Ti, and P) in a primitive-mantle-normalized trace-element spider diagram (Fig. 7d; Sun and McDonough, 1989)

4.2.3 Late Triassic monzogranite and granodiorite

SiO_2 contents of the monzogranites range from 72.56 to 75.92 wt%. The samples contain relatively high contents of K_2O (4.40–5.46 wt%) and total Na_2O+K_2O (8.44–9.40 wt%) and belong to the high-K calc-alkaline series (Fig. 6a; Peccerillo and Taylor, 1976). They also have contents of Al_2O_3=12.91–14.80 wt%, TFe_2O_3=0.75–1.56 wt%, CaO=0.25–0.35 wt%, MnO=0.01–0.02 wt%, and P_2O_5=0.01–0.05 wt%. Their A/CNK values range from 1.10 to 1.18, indicating that they are peraluminous (Fig. 6b; Maniar and Piccoli, 1989).

ΣREE contents of the monzogranites are 106–223 ppm. The degree of fractionation of LREEs and HREEs is very high (Fig. 7e; Sun and McDonough, 1989), with ΣLREE/ΣHREE ratios and $(La/Yb)_N$ ratios of 16.95–30.58 and 31.94–33.43, respectively. The samples exhibit slight negative Eu anomalies (Eu/Eu*=0.65–0.96), and are enriched in LILEs (e.g., Rb, K, La, and Ce) but depleted in HFSEs (e.g., Nb, Sr, Ti, and P) (Fig. 7f; Sun and McDonough, 1989).

The Late Triassic granodiorite samples have a narrow range of SiO_2 contents (66.79–68.98 wt%). They also have contents of Al_2O_3=14.58–15.18 wt%, K_2O=3.71–4.00 wt%, TFe_2O_3=3.56–4.38 wt%, CaO=2.13–2.92 wt%, MnO=0.06–0.07 wt%, and P_2O_5=0.15–0.18 wt%, and are classified as high-K calc-alkaline series in a K_2O vs. SiO_2 diagram (Fig. 6a; Peccerillo and Taylor, 1976). They have A/CNK ratios ranging from 0.95 to 1.01, indicating metaluminous granites (Fig. 6b; Maniar and Piccoli, 1989).

ΣREE contents of the granodiorites are 148–232 ppm, higher than the average value of continental crust (154.7 ppm). LREEs are enriched relative to HREEs, with ΣLREE/ΣHREE ratios and $(La/Yb)_N$ ratios of 11.99–12.89 and 11.50–13.97, respectively. The samples exhibit moderate negative Eu anomalies (Eu/Eu*=0.45–0.62) (Fig. 7e; Sun and McDonough, 1989), and display enrichment of LILEs and depletion in HFSEs, with negative Nb, Sr, P, and Ti anomalies and positive Nd, Zr, and Hf anomalies (Fig. 7f; Sun and McDonough, 1989).

5 Discussion

5.1 Early Mesozoic magmatism in the Chifeng area

5.1.1 Early Triassic (250–248 Ma)

Early Triassic granitic magmatism in the study area was a continuation of late Permian magmatism within the same tectonic setting (Zhang et al., 2009c; Zhang et al., 2010). The Early Triassic granitic plutons in the Chifeng area are the 250 Ma MGYZ fine-grained syenogranite, the 250 Ma XXJ syenogranite, and the 248 Ma DLG syenogranite. Other magmatic rocks of this period in the study area include the late Permian 256 Ma Shangchaoyanggou weak gneissic granite, 255 Ma Qixieyingzi syenogranite, 253 Ma Erdaogou monzogranite (Chen, 2018), and 256 Ma Chaihuyingzi diorite (Shao et al., 2012), and the Early Triassic 250 Ma Menguyingzi granodiorite (Liu et al., 2015) and 249 Ma Jinchangou gold deposit gneissic monzogranite (Duan et al., 2014). These results together confirm the extensive late Permian to Early Triassic magmatic activity in the Chifeng area.

5.1.2 Middle Triassic (244–243 Ma)

Middle Triassic granitic magmatic activity recorded in the study area is scarce and is represented by isolated individual plutons. We identified the 244 Ma porphyritic granodiorite in the center of the MGYZ pluton and the 243 Ma Songshugou coarse granodiorite within the Shaoguoyingzi pluton during this study. In the northern margin of the NCC, only rare magmatic activity during the Middle Triassic is recorded, including the 244±2 Ma Fengning Yunwushan monzogranite (Zhang et al., 2014), the 241–237 Ma Jianping granite (Zhang et al., 2009c), and the 241±6 Ma Xiaofangshen gabbro (Zhang et al., 2009b) (Table 3).

5.1.3 Early Late Triassic (232–230 Ma)

Late Triassic granites are distributed mostly in the southeastern part of the study area and include the 232 Ma Bajiazi monzogranite and the 239–233 Ma Beipiaojianggoushan monzogranite (Song et al., 2010). The Ailingou porphyry-like monzogranite formed at 230 Ma, which is consistent with the crystallization age of granodiorite in this pluton (227±1 Ma, Zhang, 2013). Other Late Triassic rocks in the study area include porphyritic monzogranite and intermediate-acidic vein rocks in the Jinchangouliang gold deposit (Aohanqi), which formed at 216±1 Ma and 228±1 Ma, respectively (Table 3). The occurrence of Late Triassic granitic magmatism in the Chifeng area was a response to large-scale Late Triassic magmatic events in the northern margin of the North China Plate.

Based on our zircon U-Pb age data and results of previous studies, the Triassic granitic magmatism of the Chifeng area can be divided into three stages: Early Triassic (250–248 Ma), Middle Triassic (244–243 Ma), and early Late Triassic (232–230 Ma).

5.2 Genetic types of Triassic granitic rocks from the Chifeng area

5.2.1 Early Triassic syenogranites

The Early Triassic syenogranites, represented by the XXJ and DLBG plutons, have high Si and total Na_2O+K_2O contents and Na_2O/K_2O ratios of 0.60–1.30, indicating characteristics of alkali-rich, calc-alkaline rocks. Their A/CNK values range from 0.87 to 1.06, showing transitional characteristics from metaluminous to weakly peraluminous. ΣREE contents of the syenogranites

are lower than the average continental crust value, and they have moderate Eu negative anomalies. Geochemical characteristics show that the syenogranites of this stage are classified as Al-saturated, high-K calc-alkaline series rocks, and it is therefore concluded that the intrusive rocks of this stage are similar to I-type granites. In (K_2O+Na_2O)/CaO vs. (Zr+Nb+Ce+Y) and TFeO/MgO vs. (Zr+Nb+Ce+Y) diagrams (Figs. 8a, 8b), the Early Triassic syenogranite samples plot mostly in the fields of FG and OGT (Figs. 8a, 8b). In $(La/Yb)_N$ vs. Yb_N and Y vs. Sr/Y diagrams (Figs. 8c, 8d), all of the samples plot in the island-arc field. Considering all the above, the Early Triassic syenogranites are considered to be high-K I-type granites.

Table 3 Geochronological data for the Triassic granitic rocks in the Chifeng area

Order	Sample	Pluton	Lithology	Age (Ma)	Method	References
1	T101	Mengguyingzi	syenogranite	250	LA-ICPMS	This study
2	D2711-1	Xiaxinjing	syenogranite	250	LA-ICPMS	This study
3	PM210-6-1	Daluobogou	syenogranite	247	LA-ICPMS	This study
4	PM101-7-2	Mengguyingzi	Granodiorite	244	LA-ICPMS	This study
5	D2493-1	Songshugouliang	Granodiorite	243	LA-ICPMS	This study
6		Bajiazi	Monzogranite	234	LA-ICPMS	Regional geological survey
7	T409		Monzogranite	232	LA-ICPMS	This study
8	14CH14	Ailingou	Granodiorite	230	LA-ICPMS	This study
9		Ailingou	Granodiorite	228	LA-ICPMS	Zhang, 2013
10		Xitaizi	Monzogranite	214	LA-ICPMS	Regional geological survey
11	PM023-17	Xitaizi	Monzogranite	209	LA-ICPMS	Regional geological survey
12	GSJ2	Jichanggouliang	Diorite	228	LA-ICPMS	Fu et al., 2010
13	PM025-7	Jianggoushan	Monzogranite	239	LA-ICPMS	Song et al., 2010
14	PM023-16	Jianggoushan	Monzogranite	233	LA-ICPMS	Song et al., 2010
15	HNY-2	Henanyingzi	Diorite	221	LA-ICPMS	Shao et al., 2011
16	XG01	Jichanggouliang	Monzogranite	250	LA-ICPMS	Duan et al., 2014
17	FS04	Xitaizi	Monzogranite	217	LA-ICPMS	Duan et al., 2014

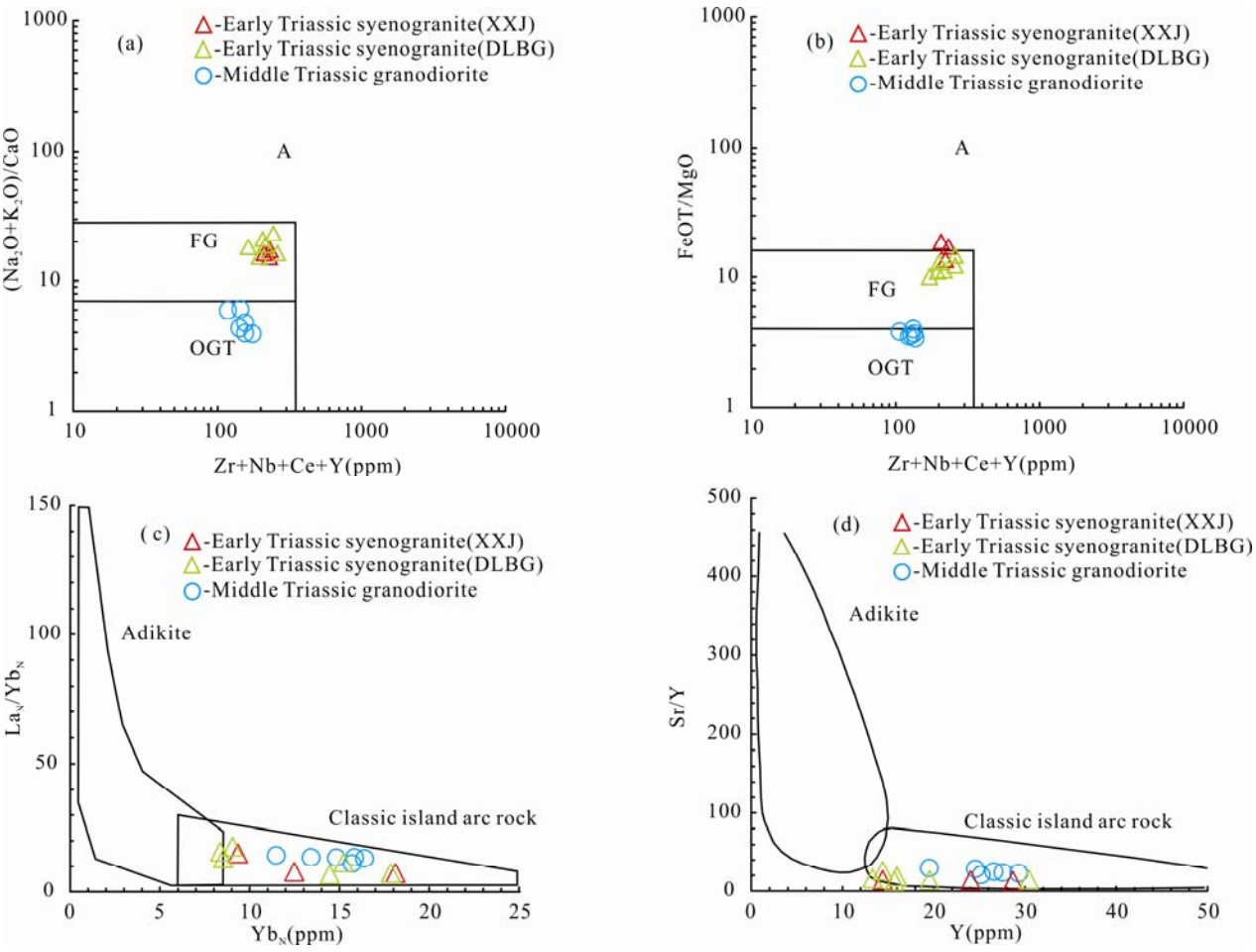

Fig. 8. Genesis diagram of the Early-Middle Triassic granites in Chifeng area

(a) Zr+Nb+Ce+Y versus $(K_2O+Na_2O)/CaO$, (b) Zr+Nb+Ce+Y versus FeO^T/MgO, after Whalen et al. (1987). A, A-type granite; FG, highly fractionated I-type; OGT, unfractionated I, S and M-type. (c) La_N/Yb_N versus Yb_N; (d) Sr/Y versus Y, after Whalen et al. (1987).

5.2.2 Middle Triassic granodiorites

The Middle Triassic acidic intrusive rocks are distributed predominantly in the MGYZ and SSLG plutons and are composed chiefly of granodiorites. Geochemically, the granodiorites are characterized by high SiO_2 (64.48–67.41 wt%), Al_2O_3 (15.48–16.08 wt%), MgO (1.45–2.00 wt%), and Sr (507.96–671.55 ppm) contents, high $(La/Yb)_N$, slight negative Eu anomalies, and low HFSE (e.g., Nb and Ta) contents; these geochemical features are similar to those of adakites (Zhang, 2001, 2004; Defant et al., 2002; Paterno, 2006). However, the granodiorites have high Y (19.54–29.32 ppm) and Yb (2.30–2.76 ppm) contents, low Sr/Y (20.05 ppm) contents, and weak negative Sr anomalies. In Y vs. Sr/Y and Yb_N vs. $(La/Yb)_N$ diagrams (Figs. 8c, 8d), none of the granodiorite samples falls in the adakite field.

The petrological and geochemical characteristics of the granodiorites suggest that they are quasi-aluminous, moderately alkaline, high-K calc-alkaline series rocks, with Na_2O/K_2O ratios and A/CNK values of 1.30–1.38 and 0.92–0.97, respectively. REE contents are higher than the average value of continental crust. Eu shows moderate negative anomalies, consistent with I-type granite. In (Zr+Nb+Ce+Y) vs. TFeO/MgO and (Zr+Nb+Ce+Y) vs. (K_2O+Na_2O) diagrams (Figs. 8a, 8b), the granodiorites plot mostly in the boundary region of the undifferentiated I-, S-, and M-type granites and A-type granite. Furthermore, in diagrams of Zr, Nb, Ce, and Y vs. SiO_2 (Fig. 9), all the samples fall in the I-type granite domain. Considering all the above, the Middle Triassic granodiorites are high-K I-type granites, although they have a certain similarity to adakitic rocks.

5.2.3 Late Triassic granites

The Late Triassic Bajiazi monzogranite is rich in Si and poor in Al, with higher total Na_2O+K_2O contents, Na_2O/K_2O ratios of 0.59–0.99, and A/CNK ratios of 1.09–1.18, and the corundum molecule (C) appears in the CIPW standard mineral calculation, which together show that the Bajiazi monzogranites are micro-peraluminous alkali-rich high-K calc-alkaline rocks. ΣREE contents are similar to the average value of continental crust, and Eu shows slight negative anomalies. Geochemical and petrological characteristics indicate that these monzogranites may be A-type granites (Zhang et al., 2012; Zhang, 2013). In geochemical discrimination diagrams proposed by Whalen et al. (1987), most samples plot in the A-type field (Fig. 10). However, the BJZ monzogranite samples have higher Al_2O_3 contents (12.91–14.80 wt%) and show only weak/negligible negative Sr and Ba anomalies. These geochemical characteristics differ substantially from those of A-type granite (Zhang et al., 2012; Zhang, 2013) but are similar to those of evolved I-type granite.

Petrological and geochemical results show that the Late

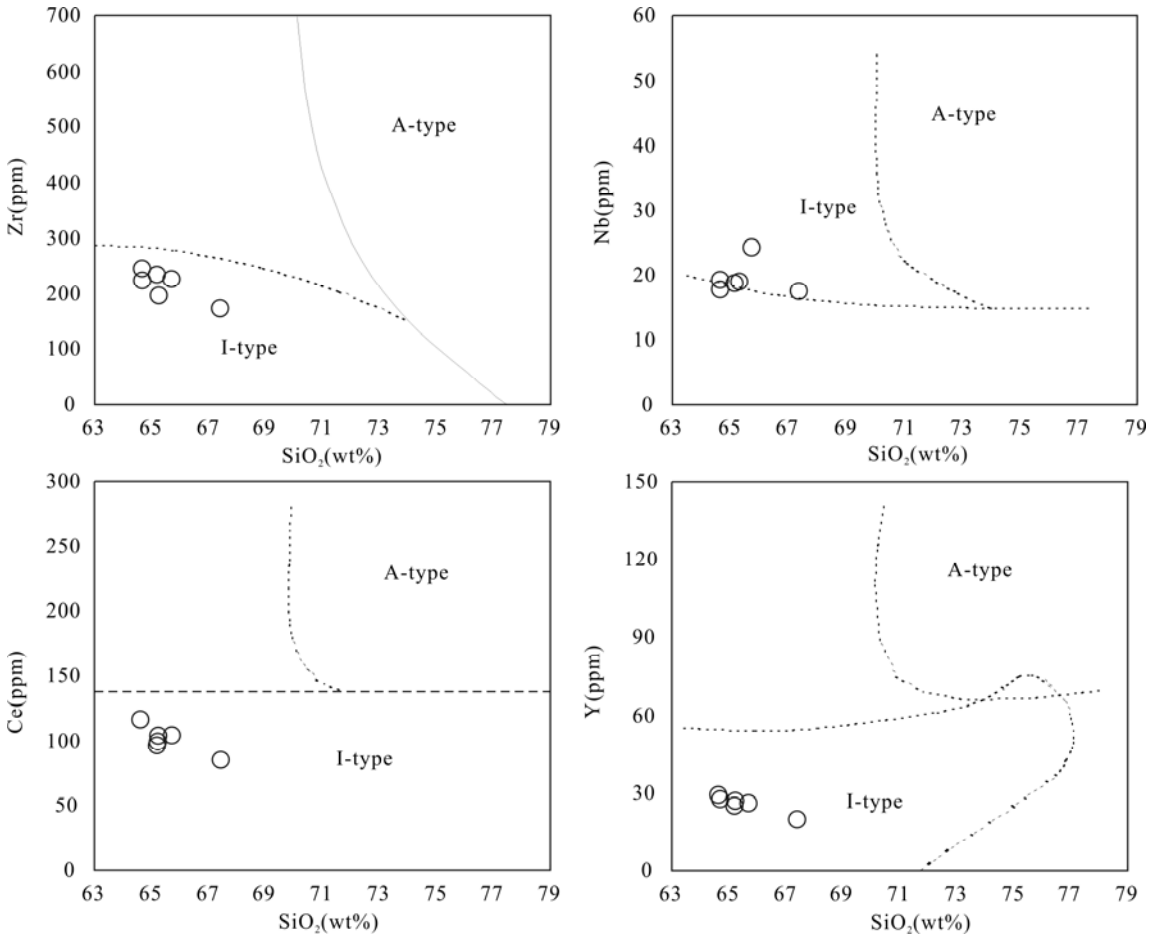

Fig. 9. Diagram of SiO_2 vs. Zr, Nb, Ce, Y for the Middle Triassic granodiorite (Collins et al.,1982).

Triassic Alingou granodiorites have medium Si and Al and low total alkali $w(Na_2O+K_2O)$ contents, Na_2O/K_2O ratios of 1.01–1.13, and A/CNK ratios of 0.95–1.01 (slightly superaluminous), and the corundum molecule (C) appears in the CIPW standard mineral calculation, which together indicate that these granodiorites are high-K calc-alkaline rocks. ΣREE contents of these granodiorite samples are higher than the average continental crust value, and Eu displays moderate negative anomalies. The samples are enriched in Rb, K, La, Ce, and other LILEs, slightly enriched in Nd, Zr, Hf, and other HFSEs, and show negative anomalies for Nb, P, Ti, and Sr. In 10,000Ga/Al-(K_2O+Na_2O)/CaO, 10,000Ga/Al-K_2O/MgO, and 10,000Ga/Al-Na_2O/K_2O diagrams, all of the samples plot in the transition zone of I-, S-, and A-type granites (Fig. 10). However, considering the SiO_2 and K_2O contents, these rocks are clearly not A-type granites (Zhang et al., 2012; Zhang, 2013).

Given all the above, we conclude that the Late Triassic Bajiazi monzogranite and the Alingou granodiorite are high-K evolved I-type granites, although they have a certain similarity to A-type granites.

5.3 Petrogenesis of Triassic high-K I-type granitic rocks from the Chifeng area

The origins of high-K calc-alkaline I-type granites are still debated (e.g., Roberts and Clemens, 1993; Liegeois et al., 1998). The existing models include 1) crustal assimilation and fractional crystallization of mantle-derived basaltic magma (e.g., DePaolo, 1981; Moghazi, 2003), 2) mixing of mantle-derived and crust-derived magmas (e.g., Dickinson, 1975; Yang et al., 2006, 2015; Clemens et al., 2009), and 3) partial melting of hydrous medium- to high-K andesitic to basaltic meta-igneous rocks under crustal conditions (e.g., Roberts and Clemens, 1993; Sisson et al., 2005; Topuz et al., 2010).

As discussed above, all three stages of Triassic granitic rocks from the Chifeng area are classified as high-K I-type granites. These rocks have high silica and alkali contents and low MgO, TFe_2O_3, CaO, and transition-element contents, as well as negative Nb, Ta, P, and Ti anomalies and positive Th, Zr, and Hf anomalies in a primitive mantle-normalized diagram. These various features suggest that the primary magma of these rocks originated from partial melting of continental crust, probably

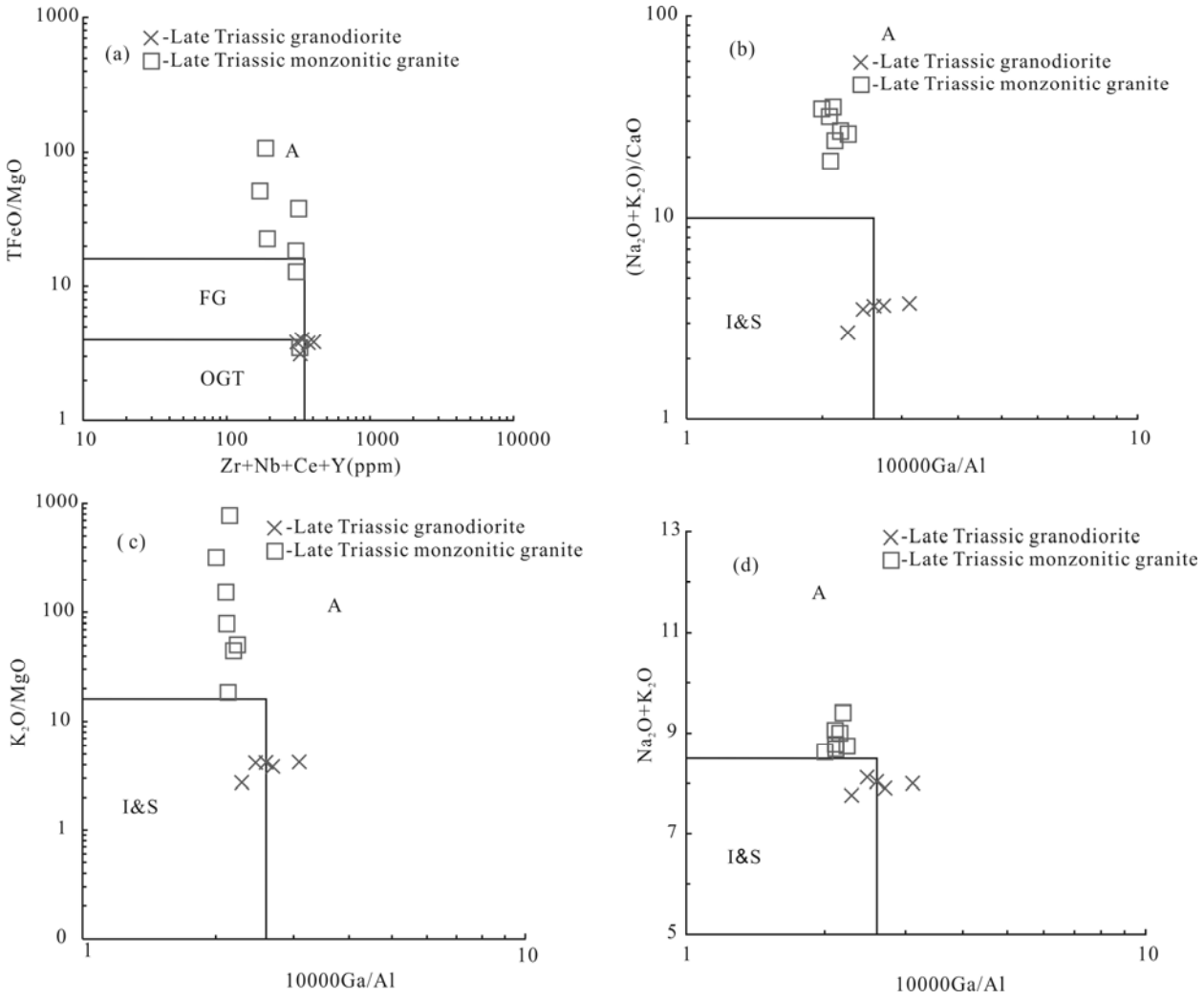

Fig. 10. Genesis diagram of the Late Triassic granites in Chifeng area.
(a) FeO^T/MgO versus Zr+Nb+Ce+Y; (b) (K_2O+Na_2O)/CaO versus 10,000Ga/Al; (c) K_2O/MgO versus 10,000Ga/Al; (d) K_2O+Na_2O versus 10,000Ga/Al, modified from Whalen et al. (1987). A, A-type granite; FG, highly fractionated I-type; OGT, unfractionated I, S and M-type.

produced by chemical differentiation of arc-derived magmas (Hofmann, 1988; Wu et al., 2007; Yu et al., 2013; Guo et al., 2014). However, the granite samples have moderate-strong negative Eu anomalies, indicating that plagioclase remained in the residue in the source or was fractionated during magmatic evolution. Moreover, all the samples contain relatively low Sr/Y ratios and high Yb and Y contents, precluding garnet in the residue (Rapp et al., 1991; Springer and Seck, 1997; Litvinovsky et al., 2000), which is consistent with the REE characteristics. These geochemical features indicate that these Triassic high-K I-type granites were derived from partial melting of a lower-crustal source at relatively low-pressure conditions.

5.4 Tectonic implications and geological significance

5.4.1 Tectonic setting

5.4.1.1 Early Triassic granites

Early Triassic magmatic rocks in the northern margin of the NCC have post-collision/post-orogenic affinity in terms of rock association, mineral composition, geochemical characteristics, magmatic evolution, and isotope composition (Zhang et al., 2010; Shao et al., 2012). The studied Early Triassic syenogranites from the Chifeng area are high-K calc-alkaline I-type granites, with enrichment in LREEs and LILEs and depletion in HFSEs, Nb, Ti, and P, showing characteristics of post-collisional granites formed in a continental orogenic belt. Tectonic environment discrimination diagrams (Figs. 11a-c, 11e, 11f) show that all of the Early Triassic granite samples plot in the post-collision granite domain. In an R1-R2 diagram (Fig. 11d), the Early Triassic granites fall mostly in the post-orogenic A-type granite domain, indicating that these rocks formed in an extensional environment, possibly related to continental-margin crustal extension (Hong et al., 1994; Eby et al., 2002; Zhang et al., 2012; Zhang, 2013). The Early Triassic granites and corresponding basalts (256–246 Ma; Miao et al., 2008; Jian et al., 2010; Chu et al., 2013; Song et al., 2016) in the study area formed bimodal volcanic rocks, all of which are distributed as an E-W-oriented strip along the northern margin of the NCC and the Xingmeng orogenic belt, further indicating an extensional environment for the Early Triassic granites in the study area.

Based on the abovementioned research results and regional geological data, the Early Triassic granites in the Chifeng area are inferred to have been emplaced in an extensional environment, most likely induced by slab break-off after final closure of the PAO along the SXCYS.

5.4.1.2 Middle Triassic granites

Our results show that the PAO in the Chifeng area closed during the Early Triassic (~248 Ma) and was followed by orogenesis. The Middle Triassic granodiorites in the Chifeng area are quasi-aluminous, medium-alkali, high-K calc-alkaline I-type granites. Tectonic environment discrimination diagrams (Figs. 11a-c, 11e, 11f) show that these rocks do not fall in the post-collision domain and

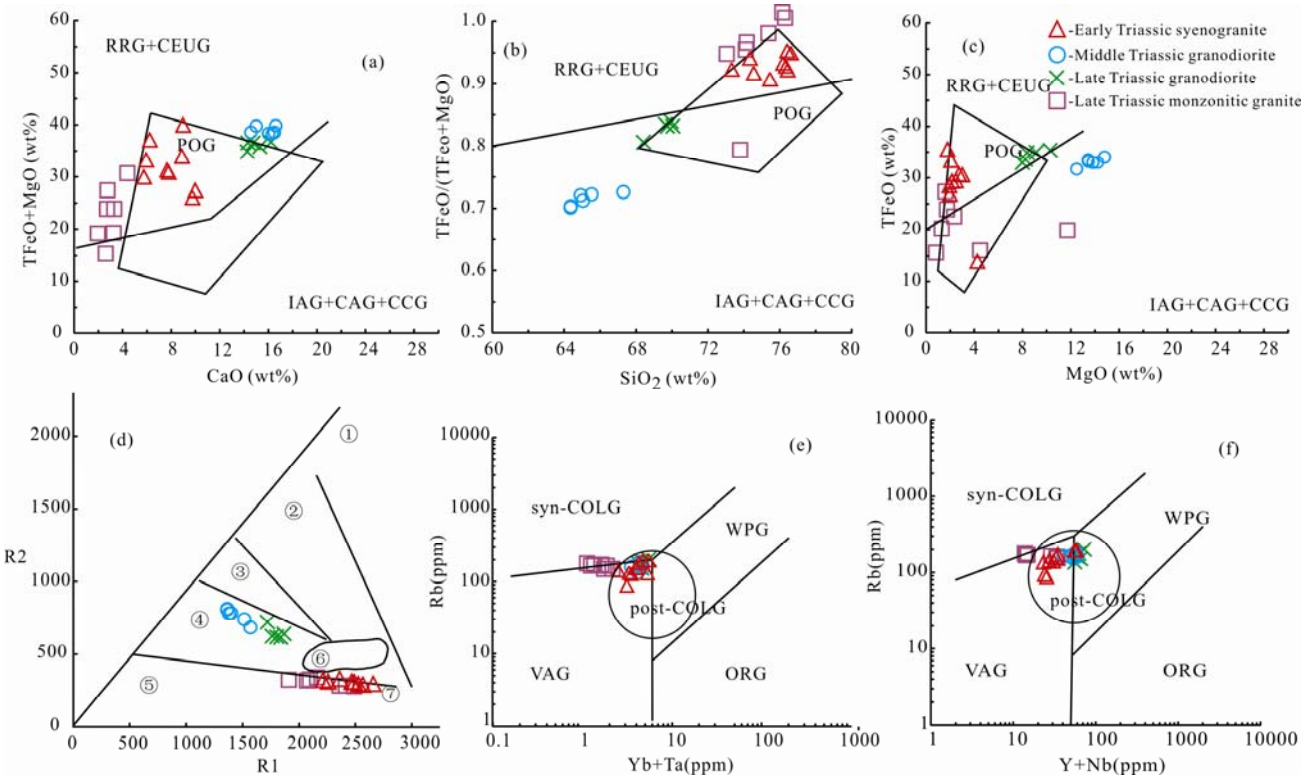

Fig. 11. Identification diagram of tectonic setting for the Triassic granites in Chifeng area.
(a) TFeO+MgO (wt%) versus CaO (wt%); (b) TFeO/(TFeO+MgO) versus SiO_2 (wt%); (c) TFeO (wt%) versus MgO (wt%), IAG, island arc granite CAG, continental arc granite CCG, continental collision granite POG, post- orogenic granite RRG, rift related granite CEUG, continental epeirogenetic uplift granite; (d) R2 versus R1, plagiogranite; active continental margin granite; collisional-orogenic granite; late orogenic granite; unorogenic A-type granite; collision granite (S-type); post-orogenic granite; (e) Rb versus Yb+Ta; (f) Rb versus Y+Nb, (after Pearce 1996), the fields are: ORG, oceanic ridge granites; syn-COLG, syn-collisional granites; VAG, volcanic arc granites; WPG, within-plate granites.

were therefore not formed in a post-collision extensional environment. In an R1-R2 diagram, the Middle Triassic granite samples plot in the domain of late orogenic granite (Fig. 11d), which indicates that the Middle Triassic granodiorite was produced during orogenesis. Therefore, the Middle Triassic granodiorites in the Chifeng area were probably emplaced in a compressive orogenic environment accompanied by collision between the Erguna-Xing'an-Songliao composite block and the NCC. The nearly E-W-oriented compressive ductile shear zone in the granodiorite pluton resulted in strong ductile shear deformation of the rock mass, implying N-S-directed compressive tectonic stress during the Middle Triassic.

5.4.1.3 Late Triassic granites

The Late Triassic rocks investigated in the study area consist of the Bajiazi monzogranite and the Ailingou granodiorite. In (Yb+Ta)-Rb and (Y+Nb)-Rb diagrams (Figs. 11e, 11f), all the Late Triassic granite samples plot in the post-collision environment domain. Geochemical characteristics indicate that the Bajiazi monzogranite is a low-pressure and strongly peraluminous granite, suggesting that it formed in a post-collision environment. In an R1-R2 tectonic environment discrimination diagram (Fig. 11d), the Ailingou I-type granite is classified as a late orogenic type granite, whereas the Bajiazi I-type granite falls in the post-orogenic A-type granite domain. This difference in classification indicates that the tectonic environment in the Chifeng area changed from a compressive orogenic to a post-orogenic extensional environment during the early Late Triassic, and then completely entered post-orogenic extension during the middle-late Late Triassic.

5.4.2 Implications for the evolution of the PAO

5.4.2.1 Early Triassic: PAO final closure and subduction slab break-off

The studied late Permian-Early Triassic granite rock association consists of A_2-subtype granite and I-type granite, with the geochemical characteristics of the association indicating that its formation was related to crustal extension of the continental margin or to intracontinental shear. These granites were formed in a post-collision environment; specifically, an extensional environment caused by slab break-off after the final closure of the PAO along the SXCYS (Fig. 12).

At present, there is strong evidence to support a late Permian-Early Triassic final closure of the PAO. Construction types, biota, and tectonic activity on opposing sides of the Xra Moron River fault during the Carboniferous-Permian differed markedly, and the paleogeographical fauna had a mixed occurrence until the middle or late Permian (Huang and Ding, 1998; Wang and Gao, 1999). In addition, the late Permian Linxi Formation and the Early Triassic Xinfuzhilu Group show no intervening unconformity, suggesting that the late Permian -Early Triassic was characterized by a continuity of tectonic setting (Deng et al., 2009; Zhang Y.S. et al., 2012; Zheng et al., 2013; Zhang et al., 2015). Furthermore, the terrestrial deposits and terrestrial animal and plant fossils of the upper Permian (Zhang et al., 2012) indicate that two major plates collided and amalgamated, generating sediments and forming the Linxi Formation (Han et al., 2011; Wang et al., 2016; Zhao et al., 2016). Radiolarians in the siliceous rocks of the Xra Moron River Formation are middle-late Permian in age (Wang, 2001). It is also thought that the final accumulation of the ophiolite belt occurred during the middle-late Permian. Both extinction events and paleomagnetic evidence indicate that closure of the PAO took place at the end of the late Permian (Li et al., 2006, 2009).

Many intrusive rocks with emplacement ages ranging from 358 to 260 Ma and composed of continental-margin arc magma are present in the northern margin of the NCC (Ma et al., 2004; Zhang et al., 2004, 2010; Wang et al., 2007; Zhang et al., 2007). The simultaneous appearance of Early Triassic post-collision A-type granites, production of bimodal volcanic rocks, and emplacement of ophiolite also indicates that the PAO disappeared and finally closed along West Lamur (Zhang et al., 2006; Miao et al., 2007; Wu et al., 2007; Peng et al., 2012; Jiang et al., 2014; Song et al., 2016).

In summary, after the initial period of collision between the Xingmeng orogenic belt and the North China Plate during the middle Permian, the late Permian-Early Triassic was characterized by gravitational collapse, and eclogite-facies metamorphism and slab break-off occurred as the subducting plate descended into the lithospheric mantle (Fig. 12a). An extensional environment developed after collision between the Xingmeng orogenic belt and the North China Plate, including in the Chifeng area, with associated underplating of the mantle source magma and upwelling of deep asthenosphere mantle. An increase in temperature and reduction in pressure occurred in the crust, forming the late Permian-Early Triassic post-collision A-type granite, bimodal volcanic rocks, and ophiolite. Simultaneously, the Linxi Formation was deposited in a lacustrine environment, as evidenced by freshwater bivalves and plant fossils in gray-black slate and shale (Han et al., 2011; Wang et al., 2016; Zhao et al., 2016), which, along with the disappearance of paleontological geographical divisions, indicates that the Early Triassic PAO basin had disappeared and that the Changchun-Yanji suture had finally closed by the Early Triassic.

5.4.2.2 Middle Triassic: continuous collisional compression after closure of the PAO

The Middle Triassic granodiorites in the Chifeng area formed as a result of extrusion that occurred during the late phase of orogenesis while the Xingmeng orogenic belt collided with the NCC. The northern margin of the North China Plate was still in a subduction or collision environment during the Middle Triassic. Sun (2013) dated a 245 Ma granite in the Aohanqi area, and Zhang (2004) dated a 245 Ma granite in the Yanji area, both of which are syn-collision granites, indicating that the two plates were still colliding during the Middle Triassic. Chen et al. (2001, 2002) constrained the age of collision-related granite in Suzuoqi at 250–230 Ma, and it is speculated that the final suture zone of the PAO in that area occurred between 310 and 230 Ma (Chen et al., 2001). Accordingly,

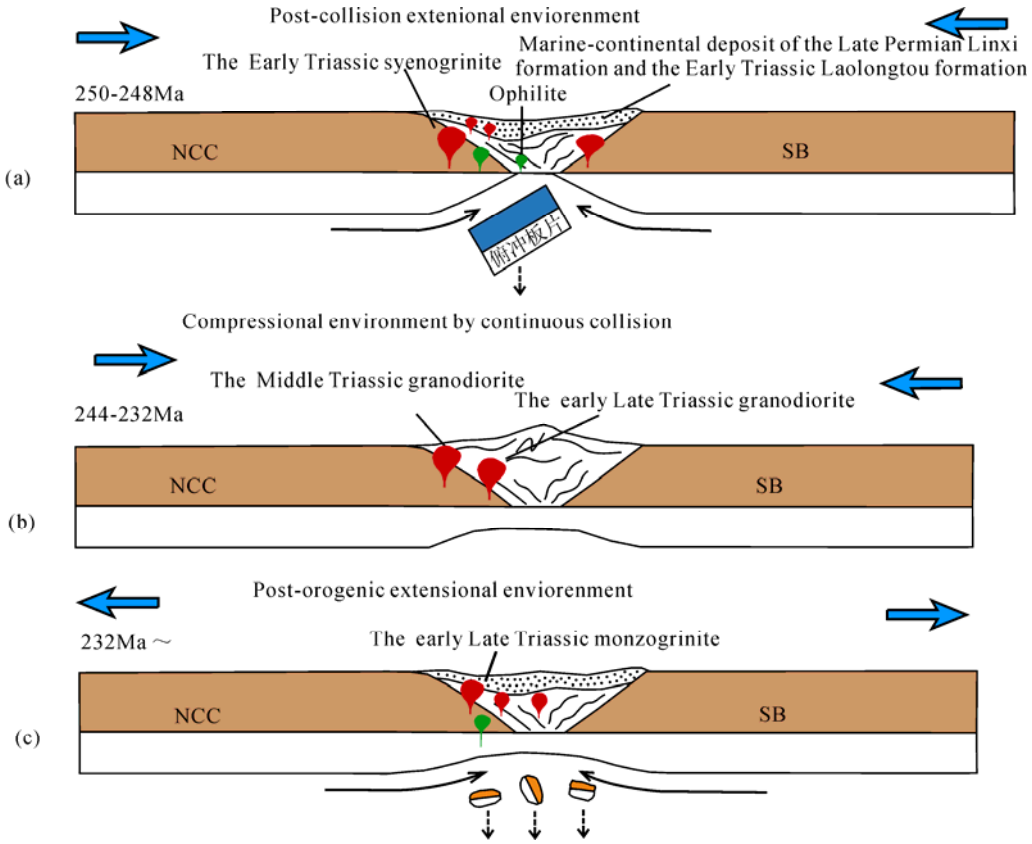

Fig. 12. A cartoon model for the tectonic evolution of the north margin of the NCC in Chifeng area during the Triassic.

NCC, North China Craton; SB, Songliao Block.

collision between the Xingmeng orogenic belt and the North China Plate continued from the middle Permian to the Middle-Late Triassic. S-type granite that was formed by young crustal re-melted magma during the Late Triassic in the Shuangjingzi area of eastern Inner Mongolia has the same collisional granite geochemistry (Li et al., 2007), which suggests that they likely formed during the late stage of collisional orogeny in that area, meaning that the two plates began to collide at about 270 Ma along the Xra Moron suture zone, with collision ending at 230 Ma (Li et al., 2007). These various lines of evidence demonstrate that the process of collision and amalgamation of the Xingmeng orogenic belt and the North China Plate was continuous during the Middle Triassic.

The Chifeng area remained under compressional collision after the final closure of the PAO during the Middle Triassic (Fig. 12b), during which both the Middle Triassic syn-collisional granodiorite reported in the present study and the monzogranite reported by Sun (2013) formed.

5.4.2.3 Late Triassic: post-orogenic extension

The record of Late Triassic magmatism in the Chifeng area is dominated by the 234 Ma Liangjianggou monzogranite (Song et al., 2010), the 232 Ma Bajiazi monzogranite, the 230–227 Ma Ailingou monzogranite (Zhang, 2013), the 228 Ma Jinchanggouliang intermediate -acidic dike (Fu et al., 2010), and the 216 Ma Xitaizi monzogranite (Duan et al., 2014). All these rocks display geochemical characteristics consistent with those of post-orogenic granites (Fig. 12c). Late Triassic magmatism in the northern margin of the North China Plate was widespread, and high-K calc-alkaline granites in central and eastern Inner Mongolia have been dated at 235 to 222 Ma (Chen et al., 2001; Luo et al., 2002, 2003; Li et al., 2007; Shao et al., 2012; Yang et al., 2012; Zhang et al., 2012; Zhang X H et al., 2012; Zhang et al., 2014). Granites formed in the Jilin-Yanbian area in the eastern part of the northern margin of the North China Plate at 235 to 224 Ma (Miao et al., 2002; Jiang et al., 2007; Zhang et al., 2012; Liu et al., 2016). The northern margin of the North China Plate hosted mafic-ultramafic intrusions, including the Huadian-Hongqiling intrusions (Cao, 2013), the Jilin Hongqiling and Piaohechuan intrusions (216–217 Ma, Wu et al., 2004), and the Xiaozhangjiakou intrusion in Chicheng (220 Ma, Tian et al., 2007). Furthermore, a Late Triassic (233–216 Ma) alkaline-complex belt is distributed as an E-W-trending strip along the northern margin of the North China Plate (Han et al., 2004; Wu et al., 2005, 2008; Ren et al., 2009; Liu et al., 2016). This alkaline-complex belt extends westward to eastern Alashan (Zhang et al., 2010) and eastward to North Korea, and the time of emplacement (234–224 Ma; Wu et al.,

2007) is very similar to that in the northern margin of the North China Plate.

There are two different understandings of the tectonic setting of the extensive Late Triassic magmatic rocks distributed in the northern margin of the North China Plate: (1) Post-collision extension in the margin of the North China Plate (Hong et al., 2000; Sun et al., 2001, 2005; Wu et al., 2002, 2004; Fu et al., 2010; Zhang X H et al., 2012; Zhang et al., 2012; Duan et al., 2014; Liu et al., 2016); and (2) post-collision extension under the background of the underlying action, causing the destruction of the NCC (Shao et al., 2000, 2011, 2012; Yang and Wu, 2009; Yang et al., 2012).

The Late Triassic igneous rock assemblage in the northern margin of the North China Plate consists of bimodal volcanic rocks and an alkaline complex, similar to the typical assemblage of a post-orogenic extensional environment. Spatially, the Late Triassic igneous rocks show an east-west distribution and are in contact with the northeastern plateau and the Xingmeng orogenic belt (Wu et al., 2002, 2004; Zhang et al., 2009c). Furthermore, extensive 230–200 Ma A-type intrusive and volcanic rocks have been recognized in the Great Xing'an Range, the Zhangguangcai Range, and the northern margin of the NCC (Wu et al., 2011). Considering that A-type granitoids form at high temperature, it is proposed that these Late Triassic A-type granitoids in NE China were related to post-orogenic evolution of the CAOB, most probably as a result of lithospheric delamination after amalgamation of the Erguna-Xing'an-Songliao composite block and the NCC (Wu et al., 2002).

6 Conclusions

Our zircon U-Pb dating and whole-rock geochemical data for Triassic granitic intrusions in the Chifeng area, Inner Mongolia Autonomous Region, allow us to draw the following conclusions:

(1) LA-ICP-MS zircon U-Pb data indicate three stages of Triassic granitic magmatism in the Chifeng area: an intrusive suite of syenogranites at 250–248 Ma, a suite of granodiorites at 244–243 Ma, and an intrusive suite of monzogranites and granodiorites at 232–230 Ma.

(2) The Chifeng Triassic granitic rocks are high-K I-type granites that were derived from partial melting of a lower-crustal source at relatively low-pressure conditions and subsequently underwent extensive fractional crystallization.

(3) The early Mesozoic tectonic evolution of the Chifeng area can be divided into three stages: closure of the Paleo-Asian Ocean and extension related to slab break-off during the Early Triassic; continuous collisional compression during the Middle Triassic after closure of the Paleo-Asian Ocean; and post-orogenic extension during the Late Triassic, most probably due to lithospheric delamination after amalgamation of the Erguna-Xing'an-Songliao composite block and the NCC.

Acknowledgements

We thank the staff of the Geologic Lab Center, China University of Geosciences (Beijing) and the Zhongnan Mineral Supervision and Testing Center of the Ministry of Land and Resources, for their advice and assistance during zircon U-Pb dating by LA-ICP-MS. We also appreciate the Northeast China Supervision and Inspection Center of Mineral Resources, Ministry of Land and Resources, Shenyang, China, for their assistance in the major and trace element analysis. This work was financially supported by the National Key Research and Development Program (Grant Nos. 2018YFC0603804) and the China Geological Survey (Grants DD20190042, DD20190039 and DD20160048-05). We thank the reviewers for their critical reviews and excellent suggestions that helped to improve an early version of this manuscript.

Manuscript received May 15, 2019
accepted Aug. 14, 2019
associate EIC XIAO Wenjiao
edited by LIU Lian

References

Andersen, T., 2002. Correction of common lead in U-Pb analyses that do not report ^{204}Pb. Chemical Geology, 192: 59–79.

Badarch, G., Cunningham, W.D., and Windley, B.F., 2002. A new terrane subdivision for Mongolia: implications for the Phanerozoic crustal growth of Central Asia. Journal of Asian Earth Sciences, 21: 87–110.

Belousova, E.A., Griffin, W.L., O'Reilly, S.Y., and Fisher, N., 2002. Igneous Zircon: Trace element composition as an indicator of source rock type. Contributions to Mineralogy and Petrology, 143(5): 602–622.

Buslov, M.M., Saphonova, I.Y., Watanabe, T., Obut, O.T., Fujiwara, Y., Iwata, K., Semakov, N.N., Sugai, Y., Smirnova, L.V., and Kazansky, A.Y., 2001. Evolution of the Paleo-Asian Ocean (Altai-Sayan Region, Central Asia) and collision of possible Gondwana-derived terranes with the southern marginal part of the Siberian continent. Geosciences Journal, 5(3): 203–224.

Cao, C.Z., Yang, F.L., Tian, C.L., and Yuan, C., 1986. The ophiolite in hegenshan district, Nei Mongol, and the position of the suture line between the Sino-Korean and Siberian Plates. In: CPPTNC Editorial Committee. Contributions to the Project of Plate Tectonics in Northern China (1). Beijing: Geological Publishing House, 64–86 (in Chinese with English abstract).

Cao, H.H., 2013. Geochronology and Geochemistry of Late Paleozoic-Early Mesozoic Igneous Rocks in the Eastern Section of the Northern Margin of the North China Plat. Jilin University, 1–171 (in Chinese with English abstract).

Chen, B., Jahn, B.M., and Tian, W., 2009. Evolution of the Solonker suture zone: Constraints from zircon U-Pb ages, Hf isotopic ratios and whole-rock Nd-Sr isotope compositions of subduction- and collision-related magmas and forearc sediments. Journal of Asian Earth Sciences, 34(3): 245–257.

Chen, B., Jahn, B.M., Wilde, S.A., and Xu, B., 2000. Two contrasting Paleozoic magmatic belts in northern Inner Mongolia, China: Petrogenesis and tectonic implications. Tectonophysics, 328(1): 157–182.

Chen, B., Zhao, G.C., and Wilde, S.A., 2001. Subduction- and Collision-related Granitoids from Southern Sonidzuoqi Inner Mongolia: Isotopic Ages and Tectonic Implications. Geological Review, 47(4): 361–367 (in Chinese with English abstract).

Chen, B., 2002. Characteristics and Genesis of the Bayan Bold Pluton in Southern Sonid Zuoqi, Inner Mongolia-Typical island arc magmatic rocks instead of adakitic rocks. Geological Review, 48(3): 261–266 (in Chinese with English abstract).

Chen, J.S., Li, B., Xing, D.H., Liu, M., Yang, J.L., Wang, Y.F.,

and Chen, H.J., 2015. Zircon U-Pb Ages and Geological Significance of the Plagioclase Amphibolite in the Baoyintu Group Eastern of Chifeng. Geological Survey and Research, 2: 81–88 (in Chinese with English abstract).

Chen, J.S., 2018. Petrogenesis of the Late Paleozoic to Early Mesozoic granites from the Chifeng region and their tectonic implication. Jilin University, 1–194 (in Chinese with English abstract).

Chu, H., Zhang, J.R., Wei, C.J., Wang, H.C., and Ren, Y.W., 2013. A new interpretation of the tectonic setting and age of meta-basic volcanics in the Ondor Sum Group, Inner Mongolia, China. Science Bulletin, 58: 3580–3587.

Clemens, J.D., Darbyshire, D.P.F., and Flinders, J., 2009. Sources of post-orogenic calcalkaline magmas: the Arrochar and Garabal Hill-Glen Fyne complexes, Scotland. Lithos, 112: 524–542.

Collins, W.J., Beams, S.D., White, A.J.R., and Chappell. B.W., 1982. Nature and origin of A-type granites with particular reference to southeastern Australia. Contributions to Mineralogy and Petrology, 80(2): 189–200.

Defant, M.J., Xu, J.F., Kepezhinskas, P., Wang, Q., Zhang, Q., and Xiao, L., 2002. Adakites: some variations on a theme. Acta Petrologica Sinica, 18: 129–142.

Deng, S.H., Wan, C.B., and Yang, J.G., 2009. Discovery of a Late Permian Angara-Cathaysia mixed flora from Acheng of Heilongjiang, China, with discussions on the closure of the Paleoasian Ocean. Science in China (D)-Earth Science, 52 (11): 1746–1755 (in Chinese with English abstract).

DePaolo, D.J., 1981. Trace element and isotopic effects of combined wallrock assimilation and fractional crystallization. Earth and Planetary Science Letters, 53: 189–202.

Dickinson, W.R., 1975. Potash-depth (K-h) relations in continental-margin and intraoceanic magmatic arcs. Geology, 3: 53–56.

Dong, Y., Ge, W.C., Zhao, G.C., Yang, H., Liu, X.W., and Zhang, Y.L., 2016. Petrogenesis and tectonic setting of the Late Paleozoic Xing'an complex in the northern Great Xing'an Range, NE China: Constraints from geochronology, geochemistry and zircon Hf isotopes. Journal of Asian Earth Sciences, 115: 228–246.

Duan, P.X., Li, C.M., Liu, C., Deng, J.F., and Zhao, G.C., 2014. Geochronology and geochemistry of the granites from the Jinchanggouliang gold deposit area in the Inner Mongolia and its geological significance. Acta Petrologica Sinica, 30(11): 3189–3202 (in Chinese with English abstract).

Eby, G.N., 1992. Chemical subdivision of the A-type granitoids: petrogenetic and tectonic implications. Geology, 20: 641–644.

Eizenhöfer, P.R., Zhao, G.C., Zhang, J., and Sun, M., 2014. Final closure of the Paleo-Asian Ocean along the Solonker Suture Zone: Constraints from geochronological and geochemical data of Permian volcanic and sedimentary rocks. Tectonics, 33 (4): 441–463.

Eizenhöfer, P.R., Zhao, G.C., Sun, M., Zhang, J., Han, Y.G., and Hou, W.Z., 2015a. Geochronological and Hf isotopic variability of detrital zircons in Paleozoic strata across the accretionary collision zone between the North China craton and Mongolian arcs and tectonic implications. Geological Society of America Bulletin, 127: 1422–1436.

EizenhöFer, P.R., Zhao, G.C., Zhang, J., Han, Y.G., Hou, W.Z., Liu, D.X., and Wang, B., 2015b. Geochemical characteristics of the Permian basins and their provenances across the Solonker Suture Zone: Assessment of net crustal growth during the closure of the Palaeo-Asian Ocean. Lithos, 224–225: 240–255.

Fan, Z.Y., 1996. The Discovery and Tectonic Significance of the Carboniferous-shell "residual sheet" in the xingshuwa, the North margin of the Xra moron River, Inner Mongolia. Geological Bulletin of China, 36(1): 58–69 (in Chinese with English abstract).

Fu, L.B., Wei, J.J., Wei, Q.R., Tan, J., Li, Y.J., Li, Y.H., Wang, M.Z., and Jiang, Y.J., 2010. Petrogenesis and Geodynamic Setting of Late Triassic Dykes of Jinchanggouliang, Eastern Inner Mongolia. Earth science-Journal of China University of Geosciences, 35(6): 933–946 (in Chinese with English abstract).

Gao, F.H., Xu, W.L., Yang, D.B., Pei, F.P., Liu, X.M., and Hu, Z.C., 2007. LA-ICP-MS zircon U-Pb dating from granitoids in southern basement of Songliao basin: constraints on ages of the basin basement. Science in China (D), 50: 995–1004.

Guo, S.Z., 1986. The determination of the time limit for the combination of the Sino-Korean plate and the Siberian plate and its biostratigraphy basis. Journal of Shenyang Institute of Geology and Mineral Resources, Chinese Academy of Geological Sciences, 14: 127–136 (in Chinese with English abstract).

Guo, J.H., Peng, P., Chen, Y., Jiao, S.J., and Windley, B.F., 2012. UHT sapphirine granulite metamorphism at 1.93–1.92 Ga caused by gabbronorite intrusions: implications for tectonic evolution of the northern margin of the North China Craton. Precambrian Research, 222–223: 124–142.

Guo, Q., Xiao, W., Hou, Q., Windley, B.F., Han, C., Tian, Z., and Song, D., 2014. Construction of late Devonian Dundunshan arc in the Beishan orogen and its implication for tectonics of southern Central Asian orogenic belt. Lithos, 184 –187: 361–378.

Han, B.F., Kagami, H., and Li, H.M., 2004. Age and Nd-Sr isotopic geochemistry of the Guangtoushan alkaline granite, Hebei province, China: implications for early Mesozoic crust-mantle interaction in North China Block. Acta Petrologica Sinica, 20(6): 1375–1388 (in Chinese with English abstract).

Han, J., Zhou, J.B., Zhang, X.Z., and Qiu, H.J., 2011. Detrital zircon U-Pb dating from sandstone of the upper Permian Linxi Formation, Linxi area, Inner Mongolia, China and its tectonic implication. Geological Bulletin of China, 30(2–3): 258–269 (in Chinese with English abstract).

He, G.Q., and Shao, J.A., 1983. confirmation and tectonic significance of early Paleozoic ophiolite formation in the Xra Moron River area of southeastern Inner Mongolia. A collection of plate tectonic texts in northern China (episode 1), Beijing: Geological Publishing House, 243–250 (in Chinese with English abstract).

Hofmann, A.W., 1988. Chemical differentiation of the Earth: the relationship between mantle, continental crust, and oceanic crust. Earth and Planetary Science Letters, 90: 297–314.

Hong, D.W., Chang, W.J., Huang, H.Z., Xiao, J.Y., Xu, H.M., and Jin, M.Y., 1994. The Permian alkaline granites in central Inner Mongolia and their geodynamic significance. Journal of Southeast Asian Earth Sciences, 10(3): 169–176.

Hong, D.W., Wang, S.G., Xie, X.L., and Zhang, J.S., 2000. Genesis of positive $\varepsilon_{Nd}(t)$ granitoids in the Da Hinggan MTS. —mongolia orogenic belt and growth continental crust. Earth Science Frontiers, 7(2): 441–456 (in Chinese with English abstract).

Hoskin, P.W.O., 2001. Rare earth element chemistry of zircon and its use as a provenance indicator. Geology, 28(7): 627–630.

HsuÈ, K.J., Wang, Q., and Hao, J., 1991. Geologic evolution of the Neomonides: a working hypothesis. Eclogae Geologicae Helvetiae, 84: 1–31.

Huang, B.H., and Ding, Q.H., 1998. The Angara Flora from Northern China. Acta Geoscientia Sinica, 19(1):97–104 (in Chinese with English abstract).

Huang, J.Q., Ren, J.S., Jiang, C.F., Zhang, Z.M., and Xu, Z.Q., 1977. The basic tectonic outline of China. Acta Geologica Sinica, 2: 117–135 (in Chinese with English abstract).

Inner Mongolia 1:500000 Aohan Banner, Daogeyingzi, Xindi and Tiejiangyingzi reogional surveys, 2015. Shenyang Institute of Geology and Mineral Resources (in Chinese with English abstract).

Jahn, B.M., Wu, F.Y., and Chen, B., 2000. Massive granitoid generation in Central Asia: Nd isotope evidence and implication for continental growth in the Phanerozoic. Episodes, 23(2): 82–92.

Jahn, B.M., 2004. The Central Asian Orogenic Belt and growth of the continental crust in the Phanerozoic. Geological Society, London, Special Publications, 226: 73–100.

Jian, P., KröNer, A., Windley, B.F., Shi, Y.R., Zhang, W., Zhang, L.Q., and Yang, W.R., 2012. Carboniferous and Cretaceous mafic-ultramafic massifs in Inner Mongolia (China): A SHRIMP zircon and geochemical study of the

previously presumed integral “Hegenshan ophiolite”. Lithos, 142–143: 48–66.
Jian, P., Liu, D.Y., KröNer, A., Windley, B.F., Shi, Y.R., Zhang, W., Zhang, F.Q., Miao, L.C., Zhang, L.Q., and Tomurhuu, D., 2010. Evolution of a Permian intraoceanic arc-trench system in the Solonker suture zone, Central Asian Orogenic Belt, China and Mongolia. Lithos, 118(1–2): 169–190.
Jian, P., Liu, D.Y., KröNer, A., Windley, B.F., Shi, Y.R., Zhang, F.Q., Shi, G.H., Miao, L.C., Zhang, W., Zhang, L.Q., and Ren, J.S., 2008. Time scale of an early to mid-Paleozoic orogenic cycle of the long-lived Central Asian Orogenic Belt, Inner Mongolia of China: Implications for continental growth. Lithos, 101(3–4): 233–259.
Jiang, N., Liu, Y.S., Zhou, W.G., Yang, J.H., and Zhang, S.H., 2007. Derivation of Mesozoic adakitic magmas from ancient lower crust in the North China craton. Geochim. Cosmochim. Acta, 71: 2591–2608.
Jiang, S.H., Liang, Q.L., Nie, F.J., and Liu, Y.F., 2014. A preliminary study of zircon LAMC-ICP-MS U-Pb ages of the Shuangjingzi complex in Linxi, Inner Mongolia. Geology in China, 41(4): 1108–1123 (in Chinese with English abstract).
Jiang, X.J., 2014. Characteristics and geological significance of Middle Permian granites in Jining area, Inner Mongolia. Jilin University, 1–84 (in Chinese with English abstract).
Khain, E.V., Bibikova, E.V., Kröner, A., Zhuravlev, D.Z., Sklyarov, E.V., Fedotova, A.A., and Kravchenko-Berezhnoy, I.R., 2002. The most ancient ophiolite of the Central Asian fold belt: U-Pb and Pb-Pb zircon ages for the Dunzhugur Complex, Eastern Sayan, Siberia, and geodynamic implications. Earth and Planetary Science Letters, 199: 311–325.
Li, D.P., Jin, Y., Hou, K.J., Chen, Y.L., and Lu, Z., 2015. Late Paleozoic final closure of the Paleo-Asian Ocean in the eastern part of the Xing-Meng Orogenic Belt: Constrains from Carboniferous-Permian (meta-) sedimentary strata and (meta-) igneous rocks. Tectonophysics, 665: 251–262.
Li, J.Y., Gao, L.M., Sun, G.H., Li, Y.P., and Wang, Y.B., 2007. Shuangjingzi middle Triassic syn-collisional crust-derived granite in the east Inner Mongolia and its constraint on the timing of collision between Siberian and Sino-Korean paleo-plates. Acta Petrologica Sinica, 23(3): 565–582 (in Chinese with English abstract).
Li, J.Y., Zhang, J., Yang, T.N., Li, Y.P., Sun, G.H., Zhu, Z.X., and Wang, L.J., 2009. Crustal tectonic division and evolution of the southern part of the North Asian orogenic region and its adjacent areas. Journal of Jilin University, 39(4): 584–605 (in Chinese with English abstract).
Li, J.Y., 1995. Intercontinental remnant sea basin and collisional orogeny between plates. Collected Works of Institute of Geology, Chinese Academy of Geological Sciences, 28: 6–14 (in Chinese).
Li, J.Y., 2006. Permian geodynamic setting of Northeast China and adjacent regions: closure of the Paleo-Asian ocean and subduction of the Paleo-Pacific plate. Journal of Asian Earth Sciences, 26(3–4): 207–224.
Li, P.W., Gao, R., Guan, Y., and Li, Q.S., 2006. Palaeogeomagnetism constraints on the final Closure time of Solonke-Linxi Suture. Journal of Jilin University, 36(5): 744–758 (in Chinese with English abstract).
Li, P.W., Gao, R., Guan, Y., and Li, Q.S., 2009. The closed times of the Paleo-Asia Ocean and the Paleo-Tethys Ocean: implication for the tectonic cause of the End-Permian mass extinction. Journal of Jilin University, 39(3): 521–527 (in Chinese with English abstract).
Li, S., Chung, S.L., Wilde, S.A., Jahn, B.M., Xiao, W.J., Wang, T., and Guo, Q.Q., 2017. Early Middle Triassic high Sr/Y granitoids in the southern Central Asian Orogenic Belt: Implications for ocean closure in accretionary orogens. Journal of Geophysical Research: Solid Earth, 122: 2291–2309.
Li, S., Chung, S.L., Wilde, S.A., Wang, T., Xiao, W.J., and Guo, Q.Q., 2016a. Linking magmatism with collision in an accretionary orogen. Scientific Reports, 6(1): 25751.
Li, S., Wilde, S.A., Wang, T., Xiao, W.J., and Guo, Q.Q., 2016b. Latest Early Permian granitic magmatism in southern Inner Mongolia, China: Implications for the tectonic evolution of the southeastern Central Asian Orogenic Belt. Gondwana Research, 29: 168–180.
Li, S., Wang, T., Wilde, S.A., and Tong, Y., 2013. Evolution, source and tectonic significance of Early Mesozoic granitoid magmatism in the Central Asian Orogenic Belt (central segment). Earth-Science Reviews, 126(11): 206–234.
Li, S., Wilde, S.A., He, Z.J., Jiang, X.J., Liu, R.Y., and Zhao, L., 2014. Triassic sedimentation and post accretionary crustal evolution along the Solonker suture zone in Inner Mongolia, China. Tectonics, 33(6): 960–981.
Li, X.H., Qi, C.S., Liu, Y., Liang, X.R., Tu, X.L., Xie, L.W., and Yang, Y.H., 2005. Petrogenesis of the Neoproterozoic bimodal volcanic rocks along the western margin of Yangtze Block: new constranits from Hf isotopes and Fe/Mn ratios. Chinese Science Bulletin, 50: 2481–2486.
Li, Y.L., Zhou, H.W., Zhong, Z.Q., Zhang, X.H., Liao, Q.A., and Ge, M.C., 2009. Collision Processes of North China and Siberian Plates: Evidence from LA-ICP-MS Zircon U-Pb Age on Deformed Granite in Xar Moron Suture Zone. Earth Science - Journal of China University of Geosciences, 34(6): 931–938 (in Chinese with English abstract).
Li, H.K., Li, H.M., and Lu, S.N., 1995. Grain zircon U-Pb age for volcanic rocks from Tuanshanzi Formation of Changcheng System and their geological implication. Geochimica, 24: 43–48 (in Chinese with English abstract).
Li, S.Z., and Zhao, G.C., 2007. SHRIMP U-Pb zircon geochronology of the Liaoji granitoids: constraints on the evolution of the Paleoproterozoic Jiao-Liao-Ji belt in the Eastern Block of the North China Craton. Precambrian Research, 158: 1–16.
Liegeois, J.P., Navez, J., Hertogen, J., and Black, R., 1998. Contrasting origin of postcollisional high-K calc-alkaline and shoshonitic versus alkaline and peralkaline granitoids: the use of sliding normalization. Lithos, 45: 1–28.
Litvinovsky, B.A., Steele, I.M., and Wickham, S.M., 2000. Silicic magma formation in overthickened crust: melting of charnockite and leucogranite at 15, 20 and 25 kbar. Journal of Petrology, 41(5): 717–737.
Liu, J., Liu, Z.H., Li, S.C., Zhao, C., Peng, Y.B., Yang, Z.J., and Dou, S.Y., 2016. Geochronology and geochemistry of Triassic intrusive rocks in Kaiyuan area of the eastern section of the northern margin of North China. Acta Petrologica Sinica, 32 (9): 2739–2756 (in Chinese with English abstract).
Liu, J., Xi, A.H., Ge, Y.H., Tang, X.Y., Xu, B.W., Wang, M.Z., and Ma, Y.J., 2015. LA-ICP-MS zircon U-Pb ages and petrogenesis of granodiorite in Mengguyingzi, Chifeng, Inner Mongolia. Geological Bulletin of China, 34(2/3): 437–446 (in Chinese with English abstract).
Liu, Y.J., Li, W.M., Feng, Z.Q., Wen, Q.B., Neubauer, F., and Liang, C.Y., 2017. A review of the Paleozoic tectonics in the eastern part of Central Asian Orogenic Belt. Gondwana Research, 43: 123–148.
Liu, Y., Liu, X.M., Hu, Z.C., Diwu, C.R., Yuan, H.L., and Gao, S., 2007. Evaluation of accuracy and long-term stability of determination of 37 trace elements in geological samples by ICP-MS. Acta Petrologica Sinica, 23: 1203–1210 (in Chinese with English abstract).
Ludwig, K.R., 2003. User's Manual for Isoplot 3.0: a Geochronological Toolkit for Microsoft Excel. Berkeley Geochronology Center Special Publication, 4: 1–70.
Luo, Z.K., Guan, K., and Miao, L.C., 2002. Dating of the dykes and altered sericite in Jiapigou gold ore belt, Jilin Province and its gold ore formation age. Geoscience, 16(1): 19–25 (in Chinese with English abstract).
Luo, Z.K., Miao, L.C., Guan, K., Qiu, Y.S., Qiu, Y.M., Mcnaughton, N.J., and Groves, D.I., 2003. SHRIMP U- Pb zircon dating of the Dushan granitic batholith and related granite- porphyry dyke, eastern Hebei Province, China, and their geological significance. Geochimica, 32(2): 173–180 (in Chinese with English abstract).
Ma, F., Mu, Z.G., and Liu, Y.L., 2004. Geochronology and Geologic Significance of the Orbicular Dioritic Rocks in Luanping, Hebei Province. Geological Review, 50(4): 360–364 (in Chinese with English abstract).

Maitre, R.W.L., 1984. A proposal by the IUGS Subcommission on the Systematics of Igneous Rocks for a chemical classification of volcanic rocks based on the total alkali silica (TAS) diagram. Journal of the Geological Society of Australia, 31(2): 243–255.

Maniar, P.D., and Piccoli, P.M., 1989. Tectonic discrimination of granitoids. Geological society of America bulletin, 101: 635–643.

Miao, L.C., Fan, W.M., Liu, D.Y., Zhang, F.Q., Shi, Y.R., and Guo, F., 2008. Geochronology and geochemistry of the Hegenshan ophiolitic complex: Implications for late-stage tectonic evolution of the Inner Mongolia-Daxinganling Orogenic Belt, China. Journal of Asian Earth Sciences, 32(5): 348–370.

Miao, L.C., Qiu, Y.M., McNaughton, N., Luo, Z.K., Groves, D., Zhai, Y.S., Fan, W.M., Zhai, M.G., and Guan, K., 2002. SHRIMP U-Pb zircon geochronology of granitoids from Dongping Area, Hebei Province, China: constraints on tectonic evolution and geodynamic setting for gold metallogeny. Ore Geology Reviews, 19: 187–204.

Miao, L.C., Zhang, F.Q., Fan, W.M., and Liu, D.Y., 2007. Phanerozoic evolution of the Inner Mongolia-Daxinganling orogenic belt in North China: Constraints from geochronology of ophiolites and associated formations. Geological Society London Special Publications, 280(1): 223–237.

Moghazi, A.M., 2003. Geochemistry and petrogenesis of a high-K calc-alkaline Dokhan Volcanic suite, South Safaga area, Egypt: the role of late Neoproterozoic crustal extension. Precambrian Research, 125: 161–178.

Mossakovsky, A.A., Ruzhentsev, S.V., Samygin, S.G., and Kheraskova, T.N., 1994. Central Asian fold belt: geodynamic evolution and formation history. Geotectonics, 27(6): 445–474.

Paterno, R.C., 2006. A review of the cause of adakite. Chinese Science Bulletin, 51(6): 617–627.

Pearce, J.A., Harris, N.B.W., and Tindle, A.G., 1984. Trace element discrimination diagrams for the tectonic interpretation of granitic rocks. Journal of Petrology, 25: 956–983.

Peccerillo, A., and Taylor, S.R., 1976. Geochemistry of Eocene calc-alkaline volcanic rocks from the Kastamonu area, northern Turkey. Contributions to mineralogy and petrology, 58: 63–81.

Pei, F.P., Xu, W.L., Yang, D.B., Zhao, Q.G., Liu, X.M., and Hu, Z.C., 2007. Zircon U-Pb geochronology of basement metamorphic rocks in the Songliao basin. Chinese Science Bulletin, 52c: 942–948.

Peng, Y.Q., Qi, C.D., Zhou, X.D., Lu, X.B., Dong, H.C., and Li, Z., 2012. Ransition from Paleo-Asian Ocean domain to circum-Pacific Ocean domain for the Ji-Hei composite orogenic belt: Time Mark and Relationship to Global Tectonics. Geology and Resources, 21(3): 261–265 (in Chinese with English abstract).

Rapp, R.P., Watson, E.B., and Miller, C.F., 1991. Partial melting of amphibolite/eclogite and the origin of Archean trondhjemites and tonalites. Precambrian Research, 51(1): 1–25.

Ren, R., Mou, B.L., Han, B.F., Zhang, L., Chen, J.F., Xu, Z., and Song, B., 2009. Zircon SHRIMP U-Pb dating of the Fanshan potassic alkaline ultramafite-syenite complex in Hebei Province,China. Acta Petrologica Sinica, 25(3): 588–594 (in Chinese with English abstract).

Ren, S.M., and Huang, B.C., 2002. Preliminary study on the Post -late Paleozoic Kinematics of the main Blocks of the Paleo-Asian Ocean. Progress in Geophysics, 22(1): 113–120 (in Chinese with English abstract).

Rickwood, P.C., 1989. Boundary lines within petrologic diagrams which use oxides of major and minor elements. Lithos, 22(4): 247–263.

Roberts, M.P., and Clemens, J.D., 1993. Origin of high-potassium, calc-alkaline, I-type granitoids. Geology, 21: 825–828.

Robinson, P.T., Zhou, M.F., Hu, X.F., Reynolds, P., Bai, W.J., and Yang, J., 1999. Geochemical constraints on the oringin of the Hegenshan Opheiolite,Inner Mongolia, China. Journal of Asian Earth Sciences, 17: 423–442.

Rudnick, R.L., Gao, S., Ling, W.L., Liu, Y.S., and McDonough, W.F., 2004. Petrology and geochemistry of spinel peridotite xenoliths from Hannuoba and Qixia, North China Craton. Lithos, 77: 609–637.

Sengör, A.M.C., Natal'in, B.A., and Burtman, V.S., 1993. Evolution of the Altaid tectonic collage and Palaeozoic crustal growth in Eurasia. Nature, 364: 299–307.

Sengör, A.M.C., and Natal'in, B.A., 1996. Paleotectonics of Asia: fragments of a synthesis[M]//Yin A, Harrison T M. The Tectonic Evolution of Asia. Cambridge: Cambrige University Press, 486–641.

Shang, Q.H., 2004. Discovery and significance of Permian radiolarian in the central and eastern parts of Inner Mongolia in the northern orogenic belt. China Science Bulletin, 9(24): 2574–2579 (in Chinese with English abstract).

Shao, J.A., Han, Q.J., and Li, H.M., 2000. Discovery of Early Mesozoic Granulite xenoliths in North China Craton.Science in China (D), 30(Z1) (in Chinese with English abstract).

Shao, J.A., and Yang, J.H., 2011. The geological corridor recording the Early Mesozoic crust-mantle evolution from Chifeng to Lingyuan. Acta Petrologica Sinica, 27(12): 3525–2792 (in Chinese with English abstract).

Shao, J.A., Zhang, Z., She, H.Q., and Liu, D.S., 2012. The discovery of Phanerozoic granulite in Chifeng area of North Craton and its implication. Earth Science Frontiers, 19(3): 187–198 (in Chinese with English abstract).

Shao, J.A., 1991. Crustal evolution in the middle part of the northern margin of the Sino-Korean plate. Beijing: Beijing University Press, 1–139 (in Chinese with English abstract).

Shi, G.H., Miao, L.C., Zhang, F.Q., Jian, P., Fan, W.M., and Liu, D.Y., 2004. Emplacement age and tectonic implications of the Xilinhot A-type granite in Inner Mongolia, China. Chinese Science Bulletin, 49(7): 723–729.

Sisson, T.W., Ratajeski, K., Hankins, W.B., and Glazner, A.F., 2005. Voluminous granitic magmas from common basaltic sources. Contrib. Miner. Petrol. 148: 635–661.

Song, S.G., Wang, M.M., Xu, X., Wang, C., Niu, Y.L., Allen, M.B., and Su, L., 2016. Ophiolites in the Xing'an-Inner Mongolia accretionary belt of the CAOB: Implications for two cycles of seafloor spreading and accretionary orogenic events. Tectonics, 34(10): 2221–2248.

Song, W.M., Bian, X.F., Xing, D.H., Tao, N., and Peng, Y.D., 2010. U-Pb zircon geochronology and geochemistry of Jianggoushan intrusion in Beipiao area, Liaoning, China. Geology and resources, 19(4): 339–345 (in Chinese with English abstract).

Springer, W., and Seck, H.A., 1997. Partial fusion of basic granulites at 5–15 kbar: implications for the origin of TTG magmas. Contributions to Mineralogy and Petrology, 127(1–2): 30–45.

Sun, D.Y., Wu, F.Y., Gao, S., and Lu, X.P., 2005. Confirmation of two episodes of A-type granite emplacement during Late Triassic and Early Jurassic in the central Jilin Province, and their constraints on the structural pattern of Eastern Jilin-Heilongjiang Area, China. Earth Science Frontiers, 12(2): 263–275 (in Chinese with English abstract).

Sun, D.Y., Wu, F.Y., Lin, Q., and Lu, X.P., 2001. Petrogenesis and crust-mantle interaction of early Yanshanian Baishishan pluton in Zhangguangcai Range. Acta Petrologica Sinica, 17 (2): 227–235 (in Chinese with English abstract).

Sun, D.Y., Wu, F.Y., Zhang, Y.B., and Gao, S., 2004. The final closing time of the west Lamulun River-Changchun -Yanji plate suture zone—Evidence from the Dayushan granitic pluton, Jilin Province. Journal of Jilin University (Earth Science Edition), 2: 174–181(in Chinese with English abstract).

Sun, S.S., and McDonough, W.F., 1989. Chemical and isotopic systematics of oceanic basalts: implications for mantle composition and processes. Geological Society, London, Special Publications, 42 (1): 313–345.

Sun, Z.J., 2013. Study on gold mineralization in Chifeng-Chaoyang area on the northern margin of North craton. Jilin University, 1–206 (in Chinese with English abstract).

Tang, K.D., Shao, J.A., Li, J.C., and Kang, Z., 2004. Nature of the Yanbian suture zone and structure of Northeast Asia.

Geological Bulletin of China, 23(9–10): 885–891 (in Chinese with English abstract).
Tang, K.D., 1990. Tectonic development of Paleozoic fold belts at the northern margin of the Sino-Korean Craton. Tectonics, 9: 249–260.
Tian, D.X., Yang, H., Ge, W.C., Zhang, Y.L., Chen, J.S., Chen, H.J., and Yun, X.Y., 2018. Petrogenesis and tectonic implications of Late Carboniferous continental arc high-K granites in the Dongwuqi area, central Inner Mongolia, North China. Journal of Asian Earth Sciences, 167: 82–102.
Tian, W., Chen, B., Liu, C.Q., and Zhang, H.F., 2007. Zircon U-Pb age and Hf isotopic composition of the Xiaozhangjiakou ultramafic pluton in northern Hebei. Acta Petrologica Sinica, 23(3): 583–590 (in Chinese with English abstract).
Topuz, G., Altherr, R., Siebel, W., Schwarz, W.H., Zack, T., Hasözbek, A., Barth, M., Satır, M., and Şen, C., 2010. Carboniferous high-potassium I-type granitoid magmatism in the Eastern Pontides: the Gümüşhane pluton (NE Turkey). Lithos, 116, 92–110.
Wang, D.D., Li, S.Z., Zhou, X.G., Liu, W.W., Lin, Y.H., Zeng, Q.N., and Zhang, W.H., 2016. SHRIMP U-Pb Dating of Detrital Zircon from the Upper Permian Linxi Formation in Eastern Inner Mongolia, and Its Geological Significance. Geological Review, 62(4): 1021–1040 (in Chinese with English abstract).
Wang, H., and Gao, R.K., 1999. Comparative study on the division of Early Permian biostratigraphy in the Mandula area of the Damao Banner in Inner Mongolia. Inner Mongolia Geology, 2: 7–20 (in Chinese with English abstract).
Wang, H.C., Zhao, F.Q., Li, H.M., Sun, L.X., Miao, L.C., and Ji, S.P., 2007. Zircon SHRIMP U-Pb age of the dioritic rocks from northern Hebei: the geological records of late Paleozoic magmatic arc. Acta Petrologica Sinica, 23(3): 597–604 (in Chinese with English abstract).
Wang, H., Wang, Y.J., Chen, Z.Y., Li, Y.X., Su, M.R., and Bai, L.B., 2005. Discovery of the Permian Radiolarians from the Bayanaobao area, Inner Mongolia. Journal of Stratigraohy, 29 (5): 368–271 (in Chinese with English abstract).
Wang, Q., and Liu, X.Y., 1986. Paleoplate tectonics between Cathasia and Angaraland in Inner Mongolia of China. Tectonics, 5(7): 1073–1088.
Wang, W.Q., 2014. Late Paleozoic tectonic evolution of the Central-northern margin of the north China Craton: constraints from zircon U-Pb ages and geochemistry of lgneous rocks in Ondor Sum-Jining area. Jilin University, 1–169 (in Chinese with English abstract).
Wang, Y.J., and Fan, Z.Y., 1997. Discovery of Permian radiolarians in ophiolite belt on northern side of Xra Moron River, Inner Mongolia, and its geological significance. Acta Palaeontological Sinica, 36(1): 58–69 (in Chinese with English abstract).
Wang, Y.J., 2001. A Review of the Study of the Palaeozoic Radiation of the Palaeozoic in China. Acta Micropalaeontological Sinica, 18(4): 313–320 (in Chinese with English abstract).
Wang, Y., Fan, Z.Y., Fang, S., and Li, B.Y., 1999. Newly discovered Geological data on the North side of Xra moron River and its tectonic significance. Inner Mongolia Geology, 1: 6–28 (in Chinese with English abstract).
Wang, Y.Q., Su, Y.Z., and Liu, E., 1997. Regional Stratigraphy in Northeastern China. China University of Geosciences Press, Wuhan, 1–175 (in Chinese with English abstract).
Whalen, J.B., Currie, K.L., and Chappell, B.W., 1987. A-type granites: geochemical characteristics, discriminatuon and petrogenesis. Contributions to Mineralogy and Petrology, 95: 407–419.
Wiedenbeck, M., Allé, P., Corfu, F., Gruffin, W.L., Meier, M., Oberli, F., Quadt, A.V., Roddick, J.C., and Spiegel, W., 1995. Three natural zircon standards for U-Th-Pb, Lu-Hf, trace element and REE analyses. Geostandards and Geoanalytical Research, 19(1): 1–23.
Wilhem, C., Windley, B.F., and Gérard, M.S., 2012. The Altaids of Central Asia: A tectonic and evolutionary innovative review. Earth-Science Reviews, 113(3–4): 303–341.
Windley, B.F., Alexeiev, D., Xiao, W.J., Kröner, A., and Badarch, G., 2007. Tectonic models for accretion of the Central Asian Orogenic Belt. Journal of the Geological Society London, 164: 31–48.
Wu, F.Y., Jahn, B.M., Wilde, S.A., and Sun, D.Y., 2000. Phanerozoic crustal growth: U-Pb and Sr-Nd isotopic evidence from the granites in northeastern China. Tectonophysics, 328(1): 89–113.
Wu, F.Y., Sun, D.Y., Li, H.M., Jahn, B.M., and Wilde, S.A., 2002. A-type granites in northeastern China: age and geochemical constraints on their petrogenesis. Chemical Geology, 187(1): 143–173.
Wu, F.Y., Wilde, S.A., Zhang, G.L., and Sun, D.Y., 2004. Geochronology and petrogenesis of the post-orogenic Cu-Ni sulfide-bearing mafic-ultramafic complexes in Jilin Province, NE China. Journal of Asian Earth Sciences, 23: 781–797.
Wu, F.Y., Yang, J.H., and Liu, X.M., 2005. Chronological framework of Mesozoic granitic magmatism in the Liaodong Peninsula. Geological Journal of China Universities, 11(3): 305–317 (in Chinese with English abstract).
Wu, F.Y., Li, X.H., Yang, J.H., and Zhang, Y.H., 2007. Discussions on the petrogenesis of granites. Acta Petrologica Sinica, 23: 1217–1238 (in Chinese with English abstract).
Wu, F.Y., Xu, Y.G., Gao, S., and Deng, J.P., 2008. Lithospheric thinning and destruction of the North China Craton. Acta Petrologica Sinica, 24(6): 1145–1174 (in Chinese with English abstract).
Wu, F.Y., Sun, D.Y., Ge, W.C., Zhang, Y.B., Grant, M.L., Wilde, S.A., and Jahn, B.M., 2011. Geochronology of the Phanerozoic granitoids in northeastern China. Journal of Asian Earth Sciences, 41: 1–30.
Xiao, W.J., Windley, B.F., Hao, J., and Zhai, M.G., 2003. Accretion leading to collision and the Permian Solonker suture, Inner Mongolia, China: Termination of the central Asian orogenic belt. Tectonics, 22(6): 1069–1090.
Xiao, W.J., Windley, B.F., Huang, B.C., Han, C.M., Yuan, C., Chen, H.L., Sun, M., Sun, S., and Li, J.L., 2009. End-Permian to mid-Triassic termination of the accretionary processes of the southern Altaids: implications for the geodynamic evolution, Phanerozoic continental growth, and metallogeny of Central Asia. International Journal of Earth Sciences, 98(6): 1189–1217.
Xiao, W.J., Windley, B.F., Allen, M.B., and Han, C.M., 2013. Paleozoic multiple accretionary and collisional tectonics of the Chinese Tianshan orogenic collage. Gondwana Research, 23(4): 1316–1341.
Xu, B., and Chen, B., 1997. The structure and evolution of the Middle Paleozoic orogenic belt between the North China Plate and the Siberian Plate in the northern Inner Mongolia. Science in China, 27(3): 227–232 (in Chinese).
Xu, W.L., Wang, F., Pei, F.P., Meng, E., Tang, J., Xu, M.J., and Wang, W., 2013. Mesozoic tectonic regimes and regional ore-forming background in NE China: Constrains from spatial and temporal variations of Mesozoic volcanic rock associations. Acta Petrologica Sinica, 29(2): 339–353 (in Chinese with English abstract).
Yang, H., Ge, W.C., Zhao, G.C., Dong, Y., Xu, W.L., Wang, Z.H., Ji, Z., and Yu, J.J., 2015. Late Triassic intrusive complex in the Jidong region, Jiamusi-Khanka Block, NE China: geochemistry, zircon U-Pb ages, Lu-Hf isotopes, and implications for magma mingling and mixing. Lithos, 224–225, 143–159.
Yang, H., Ge, W.C., Ji, Z., Yu, Q., and Tian, D.X., 2019. Late Carboniferous to early Permian subduction-related intrusive rocks from the Huolongmen region in the Xing'an Block, NE China: new insight into evolution of the Nenjiang-Heihe suture. International Geology Review, 61(9): 1071–1104.
Yang, J.H., Wu, F.Y., Chung, S.L., Wilde, S.A., and Chu, M.F., 2006. A hybrid origin for the Yianshan A-type granite, northeast China: geochemical and Sr-Nd-Hf isotopic evidence. Lithos, 89: 89–106.
Yang, J.H., and Wu, F.Y., 2009. Triassic magmatism and its relation to decratonization in the eastern North China Craton. Science in China (D), 39(7): 910–921 (in Chinese with English abstract).
Yang, J.H., Sun, J.F., Zhang, J.H., and Wilde, S.A., 2012.

Petrogenesis of Late Triassic intrusive rocks in the northern Liaodong Peninsula related to decratonization of the North China Craton: Zircon U-Pb age and Hf-O isotope evidence. Lithos, 153(15): 108–128.

Yu, Q., Ge, W.C., Yang, H., Zhao, G.C., Zhang, Y.L., and Su, L., 2014. Petrogenesis of late Paleozoic volcanic rocks from the Daheshen Formation in central Jilin Province, NE China, and its tectonic implications: Constraints from geochronology, geochemistry and Sr-Nd-Hf isotopes. Lithos, 192–195: 116–131.

Yu, Q., Ge, W.C., Zhang, J., Zhao, G.C., Zhang, Y.L., and Yang, H., 2017. Geochronology, petrogenesis and tectonic implication of Late Paleozoic volcanic rocks from the Dashizhai Formation in Inner Mongolia, NE China. Gondwana Research, 34: 164–177.

Yu, J.J., Wang, F., Xu, W.L., Gao, F.H., and Tang, J., 2013. Late Permian tectonic evolution at the southeastern margin of the Songnen-Zhangguangcai Range Massif, NE China: Constraints from geochronology and geochemistry of granitoids. Gondwana Research, 24(2): 635–647.

Yuan, L.L., Zhang, X.H., Xue, F.H., and Liu, F.L., 2016a. Juvenile crustal recycling in an accretionary orogen: insights from contrasting Early Permian granites from central Inner Mongolia, North China. Lithos, 264: 524–539.

Yuan, L.L., Zhang, X.H., Xue, F.H., Lu, Y.H., and Zong, K.Q., 2016b. Late Permian high-Mg andesite and basalt association from northern Liaoning, North China: Insights into the final closure of the Paleo-Asian ocean and the orogen-craton boundary. Lithos, 258–259, 58–76.

Zhang, G.L., and Wu, F.Y., 2005. Geochronology significances of the post-orogenic mafic-untramafic rocks in Hongqiling area of Jilin Province, NE China. Seismology and Geology, 4: 600–608 (in Chinese with English abstract).

Zhang, H.H., Zheng, Y.J., Chen, S.W., Zhang, J., Su, F., Gong, F.H., Huang, X., and Zhen, Z., 2015. LA-ICP MS U-Pb geochronology of the Permian detrital zircons in Baarin Left Banner of Inner Mongolia and Its tectonic significance. Acta Geological Sinica, 89(10): 1703–1717 (in Chinese with English abstract).

Zhang, J.Y., 2013. The Petrological Characteristics and the Formation of the Elingou pluton in the Jiefangyingzi area, Inner Mongolia. Jilin University, 1–54 (in Chinese with English abstract).

Zhang, Q., Qin, K.Z., Wang, Y.L., Zhang, F.W., Liu, H.T., and Wang, Y., 2004. Study on adakite broadened to challenge the Cu and Au exploration in China. Acta Petrologica Sinica, 20 (2): 195–204 (in Chinese with English abstract).

Zhang, Q., Ran, A., and Li, C.D., 2012. A-type granite: what is the essence?. Acta Petrologica Et Mineralogica, 31(4): 621–626 (in Chinese with English abstract).

Zhang, Q., Wang, Y., Qian, Q., Yang, J.H., Wang, Y.L., Zhao, T.P., and Guo, G.J., 2001. The characteristics and tectonic-meatllogenic significances of the adakites in Yanshan period from eastern China. Acta Petrologica Sinica, 17(2): 236–244 (in Chinese with English abstract).

Zhang, Q., 2013. The criteria and discrimination for A-type granites: A reply to the question put forward by Wang Yang and some other persons for "A-type granite: what is the essence?". Acta Petrologica et Mineralogica, 33(2): 267–274 (in Chinese with English abstract).

Zhang, S.H., Zhao, Y., and Song, B., 2004. The late Paleozoic gneissic granodiorite pluton in early Pre-cambrian high-grade metamorphic terrains near Longhua county in northern Hebei province, north China:result from zircon SHRIMP U-Pb dating and its tectonic implications. Acta Petrologica Sinica, 20(3): 621–626 (in Chinese with English abstract).

Zhang, S.H., Zhao, Y., Song, B., Yang, Z.Y., Hu, J.M., and Wu, H., 2007. Carboniferous granitic plutons from the northern margin of the North China Block: implications for a late Palaeozoic active continental margin. Journal of the Geological Society, London, 164: 451–463.

Zhang, S.H., Zhao, Y., Liu, J.M., Hu, J.M., Song, B., Liu, J., and Wu, H., 2010. Geochronology, geochemistry and tectonic setting of the Late Paleozoic-Early Mesozoic magmatism in the northern margin of the North China Block: A preliminary review. Acta Petrologica et Mineralogica, 29(6): 824–842 (in Chinese with English abstract).

Zhang, S.H., Zhao, Y., Song, B., Hu, J.M., Liu, S.W., Yang, Y.H., Chen, F.K., Liu, X.M., and Liu, J., 2009a. Contrasting Late Carboniferous and Late Permian-Middle Triassic intrusive suites from the northern margin of the North China craton: Geochronology, petrogenesis, and tectonic implications. Geological Society of America Bulletin, 121: 181–200.

Zhang, S.H., Zhao, Y., Liu, X.C., Liu, D.Y., Chen, F.K., Xie, L.W., and Chen, H.H., 2009b. Late Paleozoic to Early Mesozoic mafic -ultramafic complexes from the northern North China Block: Constraints on the composition and evolution of the lithospheric mantle. Lithos, 110: 229–246.

Zhang, S.H., Zhao, Y., Kroner, A., Liu, X.M., Xie, L.W., and Chen, F.K., 2009c. Early Permian plutons from the northern North China Block: constraints on continental arc evolution and convergent margin magmatism related to the Central Asian Orogenic Belt. International Journal of Earth Sciences, 98(6): 1441–1467.

Zhang, S.H., Zhao, Y., Ye, H., Hou, K.J., and Li, C.F., 2012. Early Mesozoic alkaline complexes in the northern North China Craton: Implications for cratonic lithospheric destruction. Lithos, 155: 1–18.

Zhang, S.H., Zhao, Y., Davis, G.A., Ye, H., and Wu, F., 2014. Temporal and spatial variations of Mesozoic magmatism and deformation in the North China Craton: Implications for lithospheric thinning and decratonization. Earth-Science Reviews, 131: 49–87.

Zhang, X.H., Zhang, H.F., Tang, Y.J., and Liu, J.M., 2006. Early Triassic A-type felsic volvanism in the Xinlinhaote - Xiwuqi, central Inner Mongolia: Age, geochemistry and tectonic implications. Acta Petrologica Sinica, 22(11): 2769–2780 (in Chinese with English abstract).

Zhang, X.H., Wilde, S.A., Zhang, H.F., Tang, Y.J., and Zhai, M.G., 2009a. Geochemistry of hornblende gabbros from Sonidzuoqi, Inner Mongolia, North China: Implication for magmatism during the final stage of suprasubduction zone ophiolite formation. International Geology Review, 51: 345–373.

Zhang, X.H., Zhang, H.F., Zhai, M.G., Wilde, S.A., and Xie, L.W., 2009b. Geochemistry of middle Triassic gabbros from northern Liaoning, North China: origin and tectonic implications. Geological Magazine, 146: 540–551.

Zhang, X.H., Zhang, H.F., Wilde, S.A., Yang, Y.H., and Chen, H.H., 2010. Late Permian to Early Triassic mafic to felsic intrusive rocks from North Liaoning, North China: petrogenesis and implications for Phanerozoic continental crustal growth. Lithos, 117: 283–306.

Zhang, X.H., Mao, Q., Zhang, H.F., Zhai, M.G., Yang, Y., and Hu, Z., 2011. Mafic and felsic magma interaction during the construction of high-K calc-alkaline plutons within a metacratonic passive margin: the early Permian Guyang batholith from the northern North China Craton. Lithos, 125: 569–591.

Zhang, X.H., Yuan, L.L., Xue, F.H., and Zhang, Y.B., 2012a. Contrasting Triassic ferroan granitoids from northwestern Liaoning, North China: magmatic monitor of Mesozoic decratonization and a craton-orogen boundary. Lithos, 144–145: 12–23.

Zhang, X.H., Gao, Y.L., Wang, Z.J., Liu, H., and Ma, Y.G., 2012b. Carboniferous appinitic intrusions from the northern North China craton: geochemistry, petrogenesis and tectonic implications. Journal of the Geological Society, 169: 337–351.

Zhang, Y.B., Wu, F.Y., Wilde, S.A., Zhai, M.G., Lu, X.P., and Sun, D.Y., 2004. Zircon U-Pb ages and tectonic implications of "Early Paleozoic" granitoids at Yanbian, Jilin Province, northeast China. The Island Arc, 13: 484–505.

Zhang, Y.S., Niu, S.W., Tian, S.G., Xing, E.Y., Su, K., Cao, J., and Wang, J.T., 2012. The discovery of conchostracan fossils in the Upper Permian Linxi Formation of Linxi area, Inner Mongolia, and its geological significance. Geological Bulletin of China, 31(9): 1394–1403 (in Chinese with English abstract).

Zhang, M.S., Peng, X.D., and Sun, X.M., 1998. The Paleozoic

tectonic geographical pattern of Northeast China. Liaoning Geology, 2: 9–96 (in Chinese with English abstract).
Zhao, Y.L., Li, W.M., Wen, Q.B., Liang, T.Y., Feng, Z.Q., Zhou, J.P., and Shen, L., 2016. Late Paleozoic tectonic framework of eastern Inner Mongolia: Evidence from the detrital zircon U-Pb ages of the Mid-late Permian to Early Triassic sandstones. Acta Petrologica Sinica, 32(9): 2807–2822 (in Chinese with English abstract).
Zhao, Y., Zhai, M.G., Chen, H., and Zhang, S.H., 2017. Paleozoic-early Jurassic tectonic evolution of North China Craton and its adjacent orogenic belts. Geology in China, 44 (1): 44–60 (in Chinese with English abstract).
Zhao, C.J., Peng, Y.J., Dang, Z.X., and Zhang, Y.P., 1996. Tectonic Framework and Crust Evolution of Eastern Jilin and Heilongjiang Provinces. Liaoning University Press, Shenyang, 1–186 (in Chinese with English abstract).
Zhao, G.C., Sun, M., Wilde, S.A., and Li, S.Z., 2005. Late Archean to Paleoproterozoic evolution of the North China Craton: key issues revisited. Precambrian Research, 1367: 172–202.
Zhao, G.C., Wilde, S.A., Sun, M., Li, S.Z., Li, X.P., and Zhang, J., 2008. SHRIMP U-Pb zircon ages of granitoid rocks in the Lüliang Complex: implications for the accretion and evolution of the Trans-North China Orogen. Precambrian Research, 160: 213–226.
Zhao, G.C., and Guo, J.H., 2012. Precambrian Geology of China: preface. Precambrian Research, 222–223: 1–12.
Zhao, G.C., and Zhai, M.G., 2013. Lithotectonic elements of Precambrian basement in the North China Craton: review and tectonic implications. Gondwana Research, 23: 1207–1240.
Zhao, G.C., 2014. Precambrian Evolution of the North China Craton. Elsevier, Amsterdam, 194 p.
Zheng, Y.J., Su, F., Chen, S.W., Zhang, J., Huang, X., and Gong, F.H., 2013. New discovery of fossils in the Lower Triassic Xingfuzhilu Formation, Bairin Right Banner, Inner Mongolia. Geological Bulletin of China, 32(9): 1423–1435 (in Chinese with English abstract).

About the first author

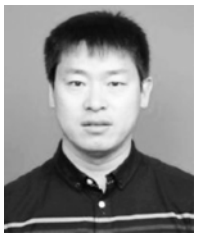

CHEN Jingsheng, male, born in 1983 in Daqing City, Heilongjiang Province; doctoral candidate and Senior Engineer; graduated from College of Earth Sciences, Jilin University. Now working in Shenyang Geological Survey Center of China Geological Survey, engages in regional geological survey. E-mail: 5202268@qq.com. Phone: 15140020313.

About the corresponding author

TIAN Dexin, male, born in 1989 in Juye City, Shandong Province; master's degree candidate and geological engineer; graduated from College of Earth Sciences, Jilin University. Now working in Non-Ferrous Metals Geological Exploration Bureau of Zhejiang Province, engages in regional geological survey. E-mail: 2272450096@qq.com. Phone: 18204018332.